Role of micro fibres in tailoring the specific heat capacity of cementitious composites at elevated temperatures: experimental characterisation and micromechanical modelling

Tong Zhang[a,b], Meng Chen[a,*], Zhiguo Yan[b], Shuhong Wang[a], Mingzhong Zhang[c,*]

[a] School of Resources and Civil Engineering, Northeastern University, Shenyang, 110819, China

[b] College of Civil Engineering, Tongji University, Shanghai, 200092, China

[c] Department of Civil, Environmental and Geomatic Engineering, University College London, London, WC1E 6BT, UK

Abstract: The temperature dependency of specific heat capacity is crucial for thermo-mechanical analysis of fibre reinforced cementitious composites. In this study, a combined experimental and theoretical analysis was conducted to characterise the role of micro fibres in tailoring the specific heat capacity of cementitious composites at elevated temperatures. The specific heat capacity of cement mortar reinforced with four types of fibres, including polypropylene, basalt, carbon and glass fibres, was measured by means of a transient method at up to 400 °C. Based on the effective medium theory, a multiscale homogenization model was developed to predict the specific heat capacity evolution of cementitious composite with temperature from micro to macro level. The results indicate that within the measured temperature range, the addition of 2.0 vol% polypropylene and glass fibres lead to the maximum rise or drop in specific heat capacity of mortar by 8.7% and 14.1%, respectively. In addition, the thermal expansion of polymer fibre was proved to effectively enhance the specific heat capacity of mortar due to thermal expansion coupling effect. The parametric analysis suggests that stiffer inclusions with high thermal expansion govern the effective specific heat capacity coupled with thermal expansion, while the composite incorporated with softer inclusions is insensitive to the variation in thermal properties of inclusions.

Keywords: Cement-based materials; Fibre reinforced mortar; Multiscale model; Microstructure; Thermal properties

1. Introduction

An accurate estimation on thermal properties of cement-based materials is crucial for predicting the thermo-mechanical response of civil infrastructure [1–3]. As a basic thermal parameter, specific heat capacity is defined as the amount of heat absorbed or released by a unit mass of the material to increase or decrease by one degree (1 K or 1 °C) in temperature, which plays an important role in determining the building energy consumption and thermal response of massive concrete structures

* Corresponding author. Email address: mingzhong.zhang@ucl.ac.uk (M. Zhang)

[4]. At ambient temperature, the specific heat capacity of cement-based materials can be affected by the water-to-cement (w/c) ratio [5], type and volume fraction of aggregates [6], curing age [7], etc. Specifically, the w/c ratio plays a dominant role in determining the microstructure of cement matrix, which would consequently alert the thermal properties of cementitious composites [8]. At elevated temperatures, the thermal properties of mortar also evolve with the changes in moisture content, phase composition and the interplay between the thermal properties of reinforced inclusions and cement matrix [9,10], while such temperature dependency is not explicitly considered in high-temperature structural design. Previous studies [11,12] revealed that the change in specific heat capacity would alter the temperature gradient and thermal stress within an order of magnitude, indicating that it is vital to explore the evolution of specific heat capacity with temperature.

In last decades, various types of synthetic and natural fibres have been widely used to improve the strength and toughness of mortar and concrete [13–15], among which polypropylene (PP) and glass fibres are mainly incorporated to enhance the deformation capability [16,17], while basalt and carbon fibres play more important roles in improving the stiffness capability [18,19]. In addition to mechanical properties, experimental results also indicated that the addition of fibres can affect the thermal properties of mortar at various temperatures [20,21]. For instance, Borinaga-Treviño et al. [22] studied the effect of recycled brass fibre on the thermal conductivity of mortar under fibre content of 0.5 to 4.0 vol% and found a maximum of 53% rise in thermal conductivity induced by brass fibre. It was reported that the high-conducting carbon fibres have a promoting effect on the thermal conductivity of mortar, while the low-conducting glass fibres would restrain the effective thermal conductivity over the temperature range of 20–400 ºC [23]. A study on the thermal conductivity, specific heat and thermal expansion of ultra-high performance cementitious composites indicated that the thermal properties were more sensitive to temperature in the presence of steel fibres. Nevertheless, it is still unclear how and to what extent the micro fibres can affect the specific heat capacity of mortar at elevated temperatures.

Apart from the experimental studies, micromechanical models based on effective medium theory were developed to predict the thermal properties of cement-based materials [25]. In particular, the incorporation of Eshelby solution into effective medium theory gives advantages of estimating the effective thermal properties of multi-phase composite considering the interaction between inclusions and the matrix [23,26]. For example, Xu et al. [5] proposed a multi-phase inclusion-matrix model to estimate the effect of interfacial resistance and size effect on the thermal conductivity of aerogel mortar, which indicates a worse thermal insulating efficiency induced by finer dispersed aerogels. Zhang et al. [27] established a homogenization framework to predict the

thermal conductivity of functional mortar containing core-shell particles and estimated the effect of core-to-shell diameter ratio on the thermal performance of mortar. Honorio et al. [7] adopted the mean-field theory to investigate the thermophysical behaviour of mortar and concrete at an early age and assessed the effects of hydration degree and interface transition zone. However, the existing models only considered the thermal properties of mortar at ambient temperature while an effective model for accurately predicting the temperature dependency of specific heat capacity from the perspective of composite theory is still lacking.

The main purpose of this study is to experimentally and theoretically investigate the effects of PP, basalt, carbon and glass fibres on the specific heat capacity of cementitious composites at elevated temperatures. Firstly, the specific heat of micro fibre reinforced mortar as a function of temperature at up to 400 ^{o}C was measured using a transient thermal analyser. Afterwards, a thermo-mechanical specific heat capacity model was developed for multi-phase composites accounting for the thermal expansion coupling effect, which was then applied to predict the thermal evolution of fibre reinforced mortar with temperature through step-by-step homogenization. The predictions were validated with experimental data. Lastly, a parametric study was conducted to estimate the effects of different factors on the macroscopic thermal properties of fibre reinforced mortar, based on which the microstructural mechanism was discussed in depth.

2. Experimental program

2.1 Raw materials

The raw materials used for cement mortar included ordinary Portland cement (CEM I, 32.5 N) with a specific gravity of 3.06, river sand with a fineness modulus of 3.2 and tap water. Four types of commercially available fibres, i.e., PP, basalt, carbon, and glass fibres, with the same fibre length of 6.0 mm were incorporated respectively to make fibre reinforced mortar. The key physical properties of these fibres at ambient temperature are given in Table 1.

Table 1 Physical properties of fibres used in this study.

Fibre type	Density (g/cm^3)	Diameter (mm)	TS (MPa)	CTE ($\times10^{-6}$ /^{o}C)	Specific heat (J/kg^{o}C)
PP	0.91	12	276	90	1680
Basalt	2.63	14	4475	7.3	940
Carbon	1.78	15	3500	0.74	712
Glass	2.54	17	1500	4.8	670

Note: TS and CTE denote the tensile strength and coefficient of thermal expansion, respectively.

2.2 Mix proportion

In total, three cement mortar mixtures with w/c ratios of 0.3, 0.4 and 0.5 were adopted as the control

groups, namely CM03, CM04 and CM05. CM specimens were designed to study the effect of w/c ratio on the specific heat capacity of mortar and provide basic thermal parameters for further comparison. To evaluate the maximum degree that micro fibres can affect the specific heat capacity of cementitious composites at elevated temperatures, the fibre volume fraction of all fibre reinforced mixtures was maintained at 2.0 vol% in accordance with the previous study [23]. In particular, 2.0 vol% PP fibres were added to the plain mixtures forming three sets of PP fibre reinforced mortar, namely PFRC03, PFRC04 and PFRC05, which were prepared and tested to estimate the combined effects of PP fibre and w/c ratio on the thermal properties of mortar. Moreover, 2.0 vol% basalt, carbon and glass fibres were separately added to cement mortar with a w/c ratio of 0.5, leading to the specimens of BFRC05, CFRC05 and GFRC05, which were adopted to explore the influence of fibre type on specific heat capacity. It is noted that the mix proportion of fibre reinforced mixtures in terms of volume fraction was kept consistent with that presented in a previous study [23], where the volume changes of cement, water and fine aggregates induced by fibres were considered. In addition, a type of polycarboxylate-based superplasticizer with 30% reducing water capability was added with a dosage of 1.0% by the mass of cement. Table 2 summarises the test variables corresponding to different sets of mixtures.

Table 2 Summary of test variables.

Mix ID	W/c ratio	Fibre volume fraction (%)				Test variable
		PP	Basalt	Carbon	Glass	
CM03	0.3	—	—	—	—	W/c ratio, Temperature (Reference)
CM04	0.4	—	—	—	—	
CM05	0.5	—	—	—	—	
PFRC03	0.3	2.0	—	—	—	W/c ratio, Temperature
PFRC04	0.4	2.0	—	—	—	
PFRC05	0.5	2.0	—	—	—	
BFRC05	0.5	—	2.0	—	—	Fibre type, Temperature
CFRC05	0.5	—	—	2.0	—	
GFRC05	0.5	—	—	—	2.0	

2.3 Specimen preparation

As per GB/T50081-2019 [28], mortar and fibre reinforced mortar specimens were fabricated using a Hobart-type mixer. Firstly, cement and river sand were pre-mixed under a dry state for 2 min to achieve good dispersion. After that, a mixture of water and polycarboxylate-based superplasticizer was added and mixed for 2 min until the mixture become flowable. For fibre reinforced mortar, accurately weighed synthetic fibres were then added in batches and mixed for another 5 min to achieve satisfied fibre dispersion. The fresh mixtures were poured into cubic plastic moulds with a

side size of 100 mm and in batches and compacted on a vibrating table. All specimens were demoulded after 24 h and then cured in a standard curing room with a constant temperature of 20 ± 1 °C and ≥ 95% relative humidity until 28 d. Finally, each cubic specimen was cut into two identical pieces and ground smooth to ensure effective specimen-to-sensor contact in specific heat capacity measurements. A schematic illustration of fibres and sample preparation for specific heat capacity measurement is given in Fig. 1a and 1b.

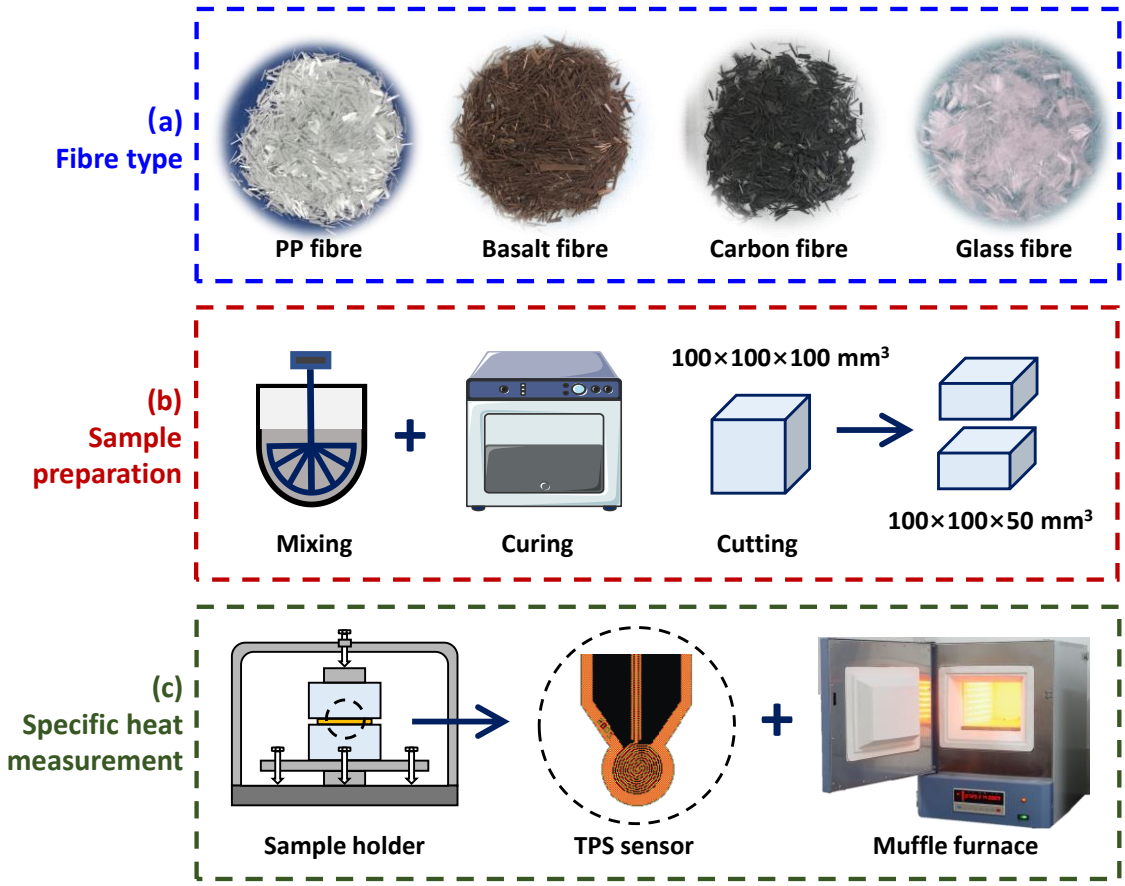

Fig. 1. Illustration of specific heat capacity measurement at elevated temperatures.

2.4 Testing methods

2.4.1 Specific heat capacity test

As per the ISO 22007-2 standard [29], the specific heat capacity of reference mortar and fibre reinforced mortar was measured using the transient plane heat source (TPS) method. The test was carried out on a commercially available thermal constant analyser, Hot Disk TPS 2500, which can be used to measure the specific heat capacity within the temperature range of 20–1000 °C. During the measurement, a Kapton plane sensor was placed between identical specimens with the dimension of 100×100×50 mm^3, and the specific heat capacity of specimens was evaluated by monitoring the thermal resistance of the transiently heated sensor. For measurement at elevated temperatures, the specimens and Kapton sensors were placed in a Muffle furnace that was

connected to and controlled by the hot disk equipment. The specimens were firstly heated to the lowest target temperature with a heating rate of 5 °C/min and kept at that temperature until reaching the thermal equilibrium state. Then, the specific heat capacity of specimens was automatically measured three times and the results were recorded by the inbuilt thermal analyser software. Afterwards, the furnace was heated again to the next target temperatures and the measurement was performed. Referring to the small-scale fire caused by the car in tunnels [30], the moderately elevated temperature of 400 ^{o}C was considered as the maximum temperature level, and the measured temperatures varied from 100 to 400 ^{o}C with an interval of 100 ^{o}C. Fig. 1c displays the setup for the specific heat capacity test.

2.4.2 Scanning electron microscope (SEM)

The microstructure of mortar and fibre reinforced specimens was characterised using a scanning electric microscope (SEM). Selected samples from the cores of specimen were cut, polished, and coated with gold for SEM imaging. A surface with multiple fibre cross-sections was needed for samples from fibre reinforced specimens. The microscopic observation was then performed using the EM 3200 SEM apparatus (KYKY, China) under the acceleration voltage of 15 kV.

3. Model development

3.1 Multiscale model of fibre reinforced cementitious composites

As a typical type of multi-phase composite, cementitious materials have complicated chemical components and inhomogeneous physical properties, whose microstructural heterogeneity manifests from nanoscale to macroscale. In this study, the multiscale microstructural characteristics of fibre reinforced cementitious composites can be divided into three lengths levels and their properties of them at each level can be achieved through step-by-step homogenization, as illustrated in Fig. 2.

Level I (10^{-6}-10^{-4} m): The representative volume element (RVE) of hardened cement paste consists of cement hydrates mainly including calcium silicate hydrate (C-S-H) gels and calcium hydroxide (CH), anhydrous cement clinkers and capillary pores. At this level, C-S-H gels are regarded as a homogeneous matrix, while the others are simplified to be spherical inclusions. The phase composition of cement paste is affected by many factors such as cement type, w/c ratio and hydration degree, which is further associated with the effective thermal properties. Herein, the Power's hydration model is adopted to estimate the effects of the w/c ratio and hydration degree.

Level II (10^{-4}-10^{-2} m): Cement mortar is composed of homogenized cement paste, sand and capillary pores/voids. It is noted that the cement paste after homogenization at Level I is regarded as the equivalent matrix at Level II, while the others are also considered as spherical inclusions. The volume fraction of each phase can be calculated based on the mix proportion of the reference mortar

and fibre reinforced mixtures as confirmed by Ref. [31]. In addition, the homogenized mortar serves as the matrix material at Level III.

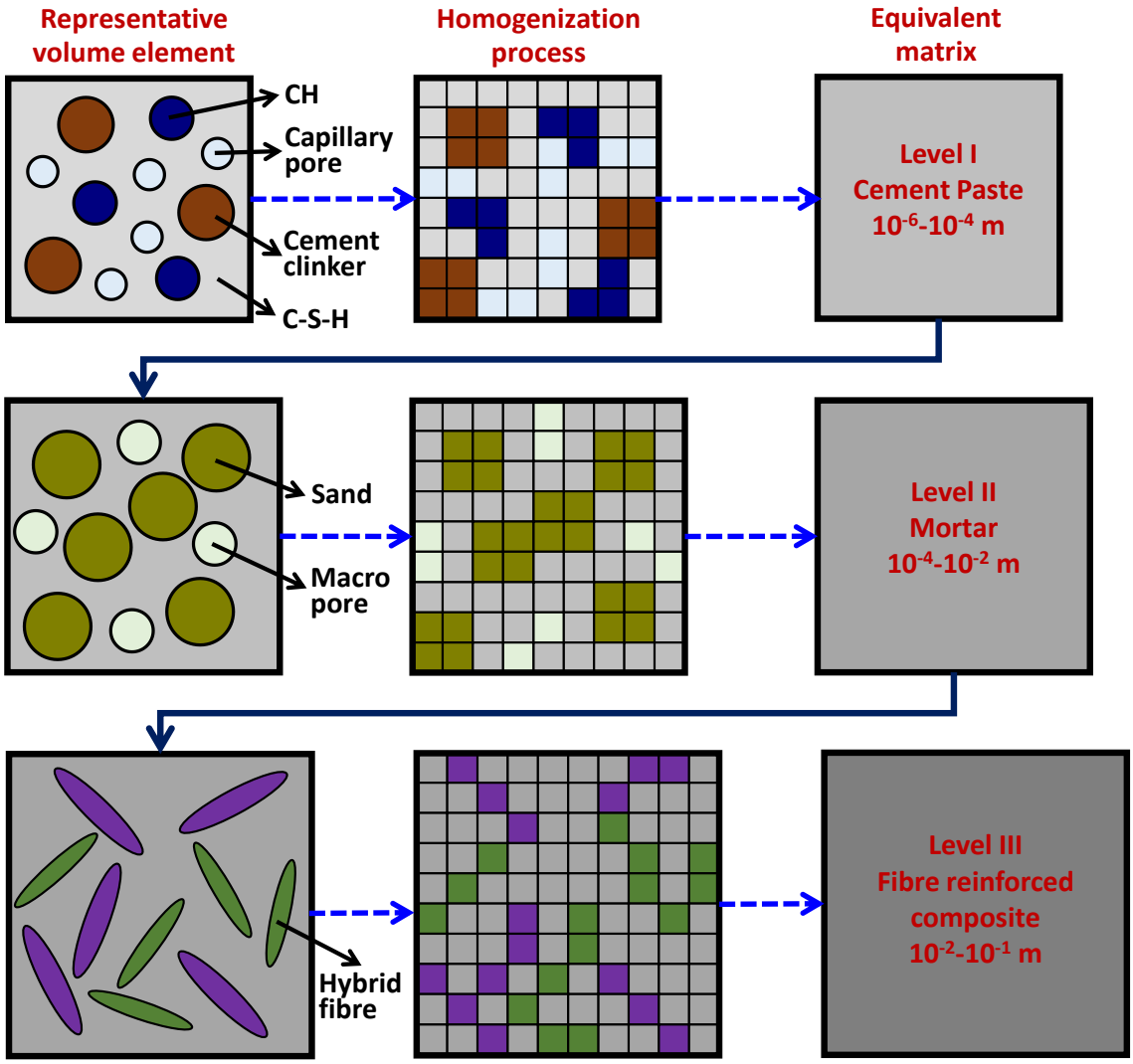

Fig. 2. Multiscale homogenization model of fibre reinforced cementitious composites.

Level III (10^{-2}-10^{-1} m): Different fibres were embedded in the homogenous matrix of cement mortar at this level. Although different types of fibres may have various dimensions, they can be simplified to ellipsoidal inclusions. In addition, previous studies suggested that the effective properties of multi-phase fibre reinforced composites are insensitive to the aspect ratio of ellipsoidal inclusions when the aspect ratio is over 10 [32]. Given that the micro fibres used in this study have an extremely high aspect ratio of more than 100, simplifications were adopted for calculations at this level in accordance with the previous study [33].

3.2 Effective specific heat capacity coupled with thermal expansion

Within the scope of thermo-elasticity, the effective thermal properties (i.e., thermal expansion and specific heat capacity) and mechanical properties (i.e., elastic modulus and stiffness) are correlated with each other. To be more specific, the thermal expansion would occur when more energy is

absorbed than the specific heat capacity during a temperature increase, while the softer the composite the lower is the resistance to thermal expansion. For the RVE of a thermoelastic composite, the volume averages of the stress tensor $\langle \boldsymbol{\sigma} \rangle$ and the strain tensor $\langle \boldsymbol{\varepsilon} \rangle$ at absolute temperature T satisfy the following entropy balance equations [34]:

$$\langle \boldsymbol{\sigma} \rangle = \overline{\boldsymbol{L}} : \left[\langle \boldsymbol{\varepsilon} \rangle - \overline{\boldsymbol{\lambda}} \left(T - T_0 \right) \right] \tag{1}$$

$$\langle \boldsymbol{\varepsilon} \rangle = \overline{\mathbb{S}} : \langle \boldsymbol{\sigma} \rangle + \overline{\boldsymbol{\lambda}} \left(T - T_0 \right) \tag{2}$$

where $\overline{\boldsymbol{\lambda}}$ stands for the effective thermal expansion tensor and T_0 denotes the reference temperature. The fourth-order effective stiffness tensor $\overline{\boldsymbol{L}}$ and compliance tensor $\overline{\mathbb{S}}$ are reciprocal of each other and can be expressed as:

$$\overline{\boldsymbol{L}} = \left(\sum_{r=0}^{N} \phi_r \boldsymbol{L}_r : \boldsymbol{A}_r^0 \right) : \left(\sum_{r=0}^{N} \phi_r \boldsymbol{A}_r^0 \right)^{-1} \tag{3}$$

$$\overline{\mathbb{S}} = \left(\sum_{r=0}^{N} \phi_r \mathbb{S}_r : \boldsymbol{B}_r^0 \right) : \left(\sum_{r=0}^{N} \phi_r \boldsymbol{B}_r^0 \right)^{-1} \tag{4}$$

where ϕ_r, $\boldsymbol{L}_r$ and $\mathbb{S}_r$ denote the volume fraction, elastic stiffness tensor and elastic compliance tensor of the rth phase, respectively, while $\boldsymbol{A}_r^0$ and $\boldsymbol{B}_r^0$ represent the rth strain and stress concentration tensor of dilute suspension.

Therefore, the second-order thermal expansion tensor can be calculated considering two types of boundary value problems [35]:

$$\overline{\boldsymbol{\lambda}} = \boldsymbol{\lambda}_0 + \sum_{r=1}^{N} \phi_r \left(\boldsymbol{\lambda}_r - \boldsymbol{\lambda}_0 \right) : \boldsymbol{B}_r \quad 69\text{-}252 \tag{5}$$

where the subscript "0" is related to the matrix, while r = (1, 2, …, N) corresponds to the rth inclusions, and $\boldsymbol{B}_r$ stands for the fourth-order stress concentration tensor.

In order to consider the effective specific heat capacity coupling with thermal expansion, the thermoelastic problem can be rewritten in terms of the effective Helmholtz free energy $\overline{H}$ as [36]:

$$\langle \rho \rangle \overline{H} = \langle \rho \rangle \overline{H_0} + \frac{1}{2} \langle \boldsymbol{\varepsilon} \rangle : \overline{\boldsymbol{L}} : \langle \boldsymbol{\varepsilon} \rangle - \langle \boldsymbol{\varepsilon} \rangle : \overline{\boldsymbol{L}} : \overline{\boldsymbol{\lambda}} \left(T - T_0 \right) - \frac{\rho_0}{2T} \overline{C_V} \left(T - T_0 \right)^2 \tag{6}$$

where $\langle \rho \rangle$ denotes the volume average density of the composite and $\overline{H_0}$ is the Helmholtz energy at a reference state relating to $\boldsymbol{\sigma} = 0$, $\boldsymbol{\varepsilon} = 0$ and $T - T_0 = 0$. Accordingly, the effective specific heat capacity of RVE at constant strain (or volume) $\overline{C_V}$ is given by:

$$\overline{C_V} \left(T - T_0 \right) = \sum_{r=0}^{N} \left\langle C_V^r \right\rangle \left(T - T_0 \right) + \frac{T}{\langle \rho \rangle} \cdot \sum_{r=0}^{N} \phi_r \left\langle \varepsilon_r \right\rangle \boldsymbol{L}_r : \boldsymbol{\lambda}_r \tag{7}$$

By substituting Eqs. (1) and (3) into Eq. (7), the effective specific heat capacity can be calculated through the superposition of boundary problems, i.e., $\boldsymbol{u}\big|_{\partial V}=0$ or $\boldsymbol{\sigma}\cdot\boldsymbol{n}\big|_{\partial V}=0$, and $T\big|_{\partial V}=T_0+\Delta T$, as [37]:

$$\begin{aligned}\overline{C_V}=&\sum_{r=0}^{N}\left\langle C_V^r\right\rangle-\frac{T}{\langle\rho\rangle}\cdot\left\{\sum_{r=0}^{N}\phi_r\boldsymbol{A}_r:\left[\sum_{i=1}^{N}\phi_i\left(\boldsymbol{L}_i^0+\boldsymbol{L}_i\right)^{-1}:\left(\boldsymbol{L}_i:\hat{\boldsymbol{\lambda}}_i-\boldsymbol{L}_0:\hat{\boldsymbol{\lambda}}_0\right)\right]:\boldsymbol{L}_r:\hat{\boldsymbol{\lambda}}_r\right\}\\&+\frac{T}{\langle\rho\rangle}\cdot\left[\sum_{r=0}^{N}\phi_r\left(\boldsymbol{L}_r^0+\boldsymbol{L}_r\right)^{-1}:\left(\boldsymbol{L}_r:\hat{\boldsymbol{\lambda}}_r-\boldsymbol{L}_0:\hat{\boldsymbol{\lambda}}_0\right):\boldsymbol{L}_r:\hat{\boldsymbol{\lambda}}_r\right]\end{aligned}\tag{8}$$

where $\boldsymbol{A}_r$ and $\boldsymbol{L}_r^0$ represent the *r*th strain concentration and strain constraint tensors, respectively.

Based on the Eshelby inclusion method and Mori-Tanaka homogenization scheme [38], the scalar thermal expansion coefficient of multi-phases composites with (*N*+1) phases can be solved from Eq. (5) as follows:

$$\overline{\lambda_{MT}}=\left[\phi_0\hat{\lambda}_0+\sum_{r=1}^{N}\frac{\phi_r\lambda_r K_r}{\chi_r K_0\left(K_r+K_0\right)}\right]\cdot\left[\phi_0+\sum_{r=1}^{N}\frac{\phi_r K_r}{\chi_r K_0\left(K_r+K_0\right)}\right]^{-1}\tag{9}$$

with

$$\chi_r=\frac{3G_0}{3K_r+4G_0}\tag{10}$$

where K_0 and K_i are the bulk modulus of the matrix and *r*th inclusion, respectively, and G_0 stands for the shear modulus of the matrix.

Accordingly, the effective specific heat capacity of thermoelastic composites can be obtained from Eq. (8) and expressed in the scalar form as:

$$\overline{C_V}=\langle C_V\rangle+\frac{9T}{\langle\rho\rangle\cdot G_0}\left[\sum_{i=1}^{N}\phi_i\chi_i\left(K_i\lambda_i-K_0\lambda_0\right)\right]\cdot\left[\sum_{r=0,i\neq r}^{N}\phi_r\chi_r\left(K_r\lambda_r-K_i\lambda_i\right)\right]\cdot\left[\sum_{r=0}^{N}\phi_r\chi_r\right]^{-1}\tag{11}$$

The first part on the right side of Eq. (11) represents the volume-averaged specific heat capacity of the matrix and inclusions, while the second part reflects the effects of thermal expansion and elastic properties on the effective specific heat capacity of the overall composite. It is noted that the final expressions of Eqs. (9) and (11) can be applied to estimate the effective thermal properties of cementitious composites at different scales, which was incorporated into the multiscale model established in Section 3.1, as illustrated in the homogenization processes in Fig. 2.

3.3 Debye specific heat capacity at elevated temperature

Driven by the lattice dynamics, the Debye model provides a direct solution to estimate the effect of elevated temperatures on the specific heat capacity of solid composites, accounting for the single frequency and broad frequency distribution of solid atoms. For example, the total energy $E(T)$ of a

solid lattice system with 3N degrees of freedom can be calculated by summing up the simple harmonic vibration of all independent lattice waves as [39]:

$$E(T)=\sum_{i=1}^{3N}\hbar w_i(q)\left(\exp\frac{\hbar w_i(q)}{\kappa_B T}-1\right)^{-1} \tag{12}$$

where $\hbar w_i(q)$ denotes the lattice wave phonons under wave vector q and frequency w_i, and κ_B stand for the Boltzmann constant, i.e., 1.3806×10^{-23} J/K.

If given the characteristic frequency w_d and defining the Debye temperature $T_d=\hbar w_d/\kappa_B$, the temperature-dependent specific heat at constant volume $C_V(T)$ can be formulated as [40]:

$$\begin{aligned} C_V(T)&=\left.\frac{\partial E}{\partial T}\right|_V=9N\kappa_B\left(\frac{T}{T_d}\right)^3\int_0^{T_d/T}\frac{\left(\hbar w/\kappa_B T\right)^4 e^{\hbar w/\kappa_B T}}{\left(e^{\hbar w/\kappa_B T}-1\right)^2}\mathrm{d}\left(\frac{\hbar w}{\kappa_B T}\right)\\ &=3N\kappa_B G\left(\frac{T_d}{T}\right)=\overline{C_V}\cdot G\left(\frac{T_d}{T}\right)\end{aligned} \tag{13}$$

where the Debye specific heat capacity function $G(\delta)$ can be estimated through Taylor series expansion and omitting the higher order terms as:

$$\begin{aligned} G\left(\frac{\vartheta_d}{T}\right)=G\left(\frac{\hbar w}{\kappa_B T}\right)&=G(\delta)\approx G(\delta)\big|_{\delta=\delta_0}+G'(\delta)\big|_{\delta=\delta_0}(\delta-\delta_0)\\ &+\frac{1}{2!}G''(\delta)\big|_{\delta=\delta_0}(\delta-\delta_0)^2+\frac{1}{3!}G'''(\delta)\big|_{\delta=\delta_0}(\delta-\delta_0)^3\end{aligned} \tag{14}$$

By embedding the homogenized $\overline{C_V}$ in Eq. (11) into Eq. (13), the evolution of effective specific heat capacity with elevated temperatures can be reflected by Debye specific heat capacity function, which will be discussed along with the predicted results below.

3.4 Additional specific heat capacity due to moisture migration

Moisture migration would inevitably alter the specific heat capacity at elevated temperatures as the specific heat capacity of water is over four times higher than that of cement paste. In this study, the energy consumed for moisture migration was regarded as the additional specific heat satisfying:

$$C_{V,all}(T)=C_V(T)+C_{add} \tag{15}$$

where $C_{V,all}(T)$ is the overall specific heat capacity of the cementitious composite, and the additional specific heat capacity C_{add} can be expressed as [41]:

$$C_{add}=\frac{H_w}{T-T_0}\left(m_{dehy}\xi_1+m_{free}\right)\xi_2 \tag{16}$$

where H_w denotes the latent heat for water evaporation, i.e., 2.26×10^6 J/kg, m_{dehy} and m_{free} stand for the weight of dehydrated water and free water, respectively. In addition, the correction factor ξ_1

is related to the energy consumed for the dehydration of hydrated products, while the correction factor ξ_2 is associated with the effect of water condensation in the cooler region.

Fig. 3 displays the relationship between Sections 3.2 to 3.4 for the illustration purpose. By combining these proposed solutions, the overall effective specific heat capacity can be calculated step by step from cement paste level to fibre reinforced cementitious composites level. Furthermore, the effectiveness and reliability of the developed multiscale model will be validated with experimental data in the following sections.

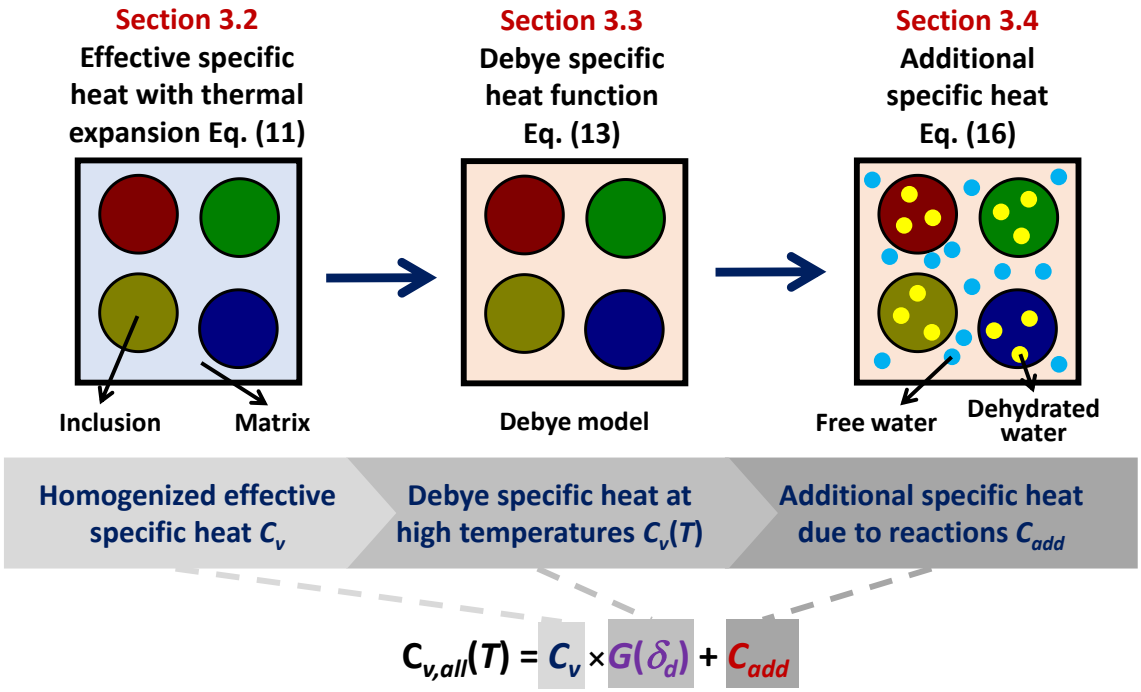

Fig. 3. Illustration for calculating the overall specific heat capacity of cementitious composites.

4. Experimental results

4.1 Specific heat capacity of cement mortar

Fig. 4a shows the measured specific heat capacity of cement mortar with various w/c ratios. It is obvious that the specific heat capacity of mortar goes up with the increasing w/c ratio, and this tendency retains throughout the measured temperature ranges. For example, the specific heat capacity of CM03 is 14.1% and 16.4% higher than that of CM05 at 20 and 400 °C, respectively. This can be mainly attributed to the increment of moisture content in cement paste with a higher w/c ratio. The previous study [42] revealed that the volume fraction of water-filled spaces in hardened cement paste with a w/c ratio of 0.5 is nearly double that with a w/c ratio of 0.3 after curing for 28 d. It is noted that the specific heat capacity of bulk water reaches up to 4.183×10^3 J/kg°C, while that of low-density (LD) and high-density (HD) C-S-H gels are only 9.46×10^2 and 9.14×10^2 J/kg°C. Accordingly, the variation of moisture content with the w/c ratio plays the dominant role in

determining the specific heat capacity of cement paste.

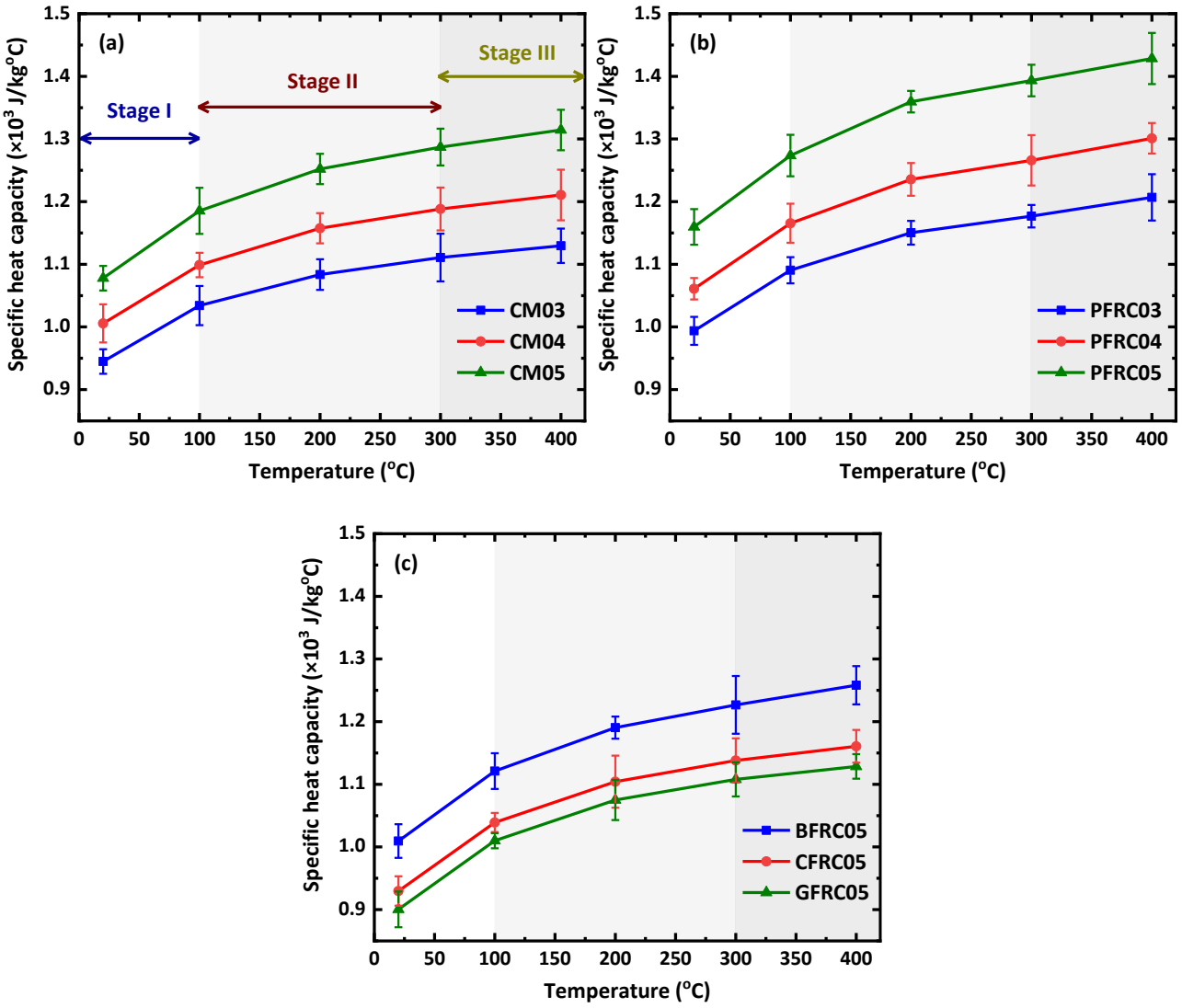

Fig. 4. Measured specific heat of mortar and fibre reinforced mortar at elevated temperatures.

When exposed to elevated temperatures, the specific heat capacity of cement mortar rises with temperature regardless of the w/c ratio, as seen in Fig. 4a. However, the growth rate of specific heat capacity gradually drops with temperatures. For sake of illustration, the measured temperature range can be divided into three stages according to the physical changes of the cement matrix [43,44] and the variation tendency of curves. The most significant increment of specific heat capacity occurs at Stage I (i.e., below 100 °C), during which the specific heat capacity of CM04 rises by 9.2%. This can be explained by the additional specific heat capacity due to the evaporation of free water at around 100 °C. In comparison with Eurocode 2 [45] where a dramatic increase to nearly the double specific heat occurred at 100 °C, the measured results in Fig. 4a indicate a smaller rise at Stage I as per previous studies [24,46]. It can be ascribed to the long holding period to reach the target temperature for TPS measurement, during which part of the moisture may already evaporate before measuring the

specific heat capacity [47,48]. At Stage II (i.e., 100–300 °C), the removal of absorbed water released by dehydration of C-S-H gels further contributes to the growth of specific heat capacity. However, the specific heat capacity of confined water in C-S-H gels is only about 27% of the free water [49], leading to a drop in the rising rate of specific heat capacity. When the temperature reaches over 300 °C, i.e., Stage III, the activation energy of decomposed C-S-H constantly increases with temperature [50], slowing down the release of confined water and reducing the additional specific heat capacity. Therefore, the specific heat capacity increment at Stage III is mainly induced by the Debye specific heat capacity of solid phases, as discussed in Section 3.3.

4.2 Specific heat capacity of PP fibre reinforced mortar

Fig. 4b displays the evolution of the specific heat capacity of PP fibre reinforced composites (PFRC) with changes in w/c ratio and exposure temperature. In alignment with CM specimens, the specific heat capacity of PFRC also rises with the increasing w/c ratio and temperatures. However, the absolute value of specific heat capacity is enhanced by incorporating PP fibres. At the ambient temperature, the specific heat capacity of PPFRC05 and PPFRC03 specimens is about 7.6% and 5.2% higher than that of cement mortar with the same w/c ratio. This can be explained by the volume averaged estimation of effective properties, i.e., the first part in Eq. (11), which is determined by means of the specific heat capacity of individual phases. The specific heat capacity of PP fibres is 1.68×10^{3} J/kg°C, nearly double that of fine aggregates, and thereby the addition of PP fibres has a promoting effect on the specific heat capacity of cement mortar. At elevated temperatures, the coefficient of linear thermal expansion of PP fibres increases from 1.0×10^{-4} to 2.1×10^{-4} ε/°C with the temperature rising from 20 to 140 °C, while the thermal expansion coefficient of cement paste maintains at below 1.5×10^{-5} ε/°C throughout the temperature range of 20–300 °C [51]. The high thermal expansion of PP fibres can also contribute to the increment in specific heat capacity of the overall composite, which corresponds to the second part in Eq. (11). Furthermore, the melting and vaporization of PP fibres at around 170 and 340 °C would also consume a certain amount of energy, resulting in an additional specific heat capacity of PFRC. Consequently, PFRC shows an abnormal regain in the increasing rate of specific heat capacity at over 300 °C, while the growth rate of CM specimens keeps reducing with temperature.

4.3 Specific heat capacity of basalt, carbon and glass fibre reinforced mortar

The effect of fibre type on the temperature-dependent specific heat capacity of cement mortar is presented in Fig. 4c. In general, the increasing tendency of specific heat with temperature remains after the addition of basalt, carbon or glass fibres, and the growing rate of the curves resembles that of CM05 specimens since no fibre melts within the measured temperature range. Additionally, the

specific heat capacity of these three types of fibre is lower than that of cement paste with a w/c ratio of 0.5, as listed in Table 1, and thus the incorporation of 2.0 vol% carbon or glass fibres causes a drop of 11.7% and 14.1% in specific heat capacity, relative to that of CM05 specimens at 400 °C. The SEM images in Fig. 5 provide more direct insight at micro scales. For cementitious matrix, the solid phases, likely to be the decomposed hydration products [44,52], were loosely packaged after heating, as shown in Fig. 5a. For fibre reinforced mortar, basalt and carbon fibres can still be observed after exposure to elevated temperatures, as seen in Fig. 5b and 5c. Moreover, there exists porous interfacial transition zone between fibres and matrix [23], which would also alter the effective thermal properties of mortar [7].

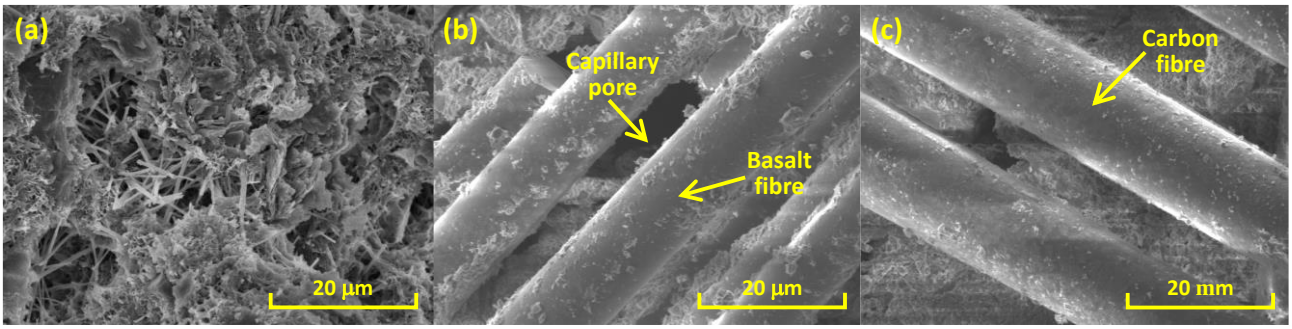

Fig. 5. SEM images of (a) cementitious matrix, and (b) and (c) fibre reinforced mortar.

5. Model validation

5.1 Homogenized specific heat capacity at Level I

As the matrix material in cement paste, C-S-H gels can be regarded as a composite of two types of hydrates with different densities, i.e., LD and HD C-S-H. In this study, the volume fraction of each gel in the matrix was calculated using the simple two-density C-S-H model [53], and the volume averaged specific heat capacity of C-S-H was used as the input thermal parameter of the matrix at Level I. The volume fractions of inclusions including cement hydrates, clinkers and pores were calculated based on the Power's hydration model, considering the synergetic effects of the w/c ratio and hydration degree [54]. Accordingly, the thermal expansion coupled specific heat capacity of cement paste can be obtained using the homogenization model proposed in Section 3.2. The basic mechanical and thermal parameters of the matrix and inclusions at Level I are listed in Table 3.

Table 3 Mechanical and thermal parameters of individual phases in cement paste at Level I [49,55].

Phase	Elastic modulus (GPa)	Poisson's ratio	CTE ($\times 10^{-6}$/K)	Specific heat (J/kg°C)
LD C-S-H	19.6	0.24	45	946
HD C-S-H	31.5	0.24	55	914
CH	40.0	0.31	70	1150
Clinker	129.4	0.30	49.5	750
Free water	—	0.50	200	4183

Confined water	—	0.50	356	1129
Air	—	—	30.7	1005

Fig. 6 displays the predicted specific heat capacity of cement paste at Level I in comparison with experimental results. To estimate the effect of inclusions on the thermal properties of the overall composite, the relative specific heat capacity which is defined as the ratio between the effective specific heat of the composite and the specific heat of the matrix material is used for comparison in the figures. In general, the predictions can be divided into three parts: (i) the volumetric average specific heat for solids, calculated based on the volume fractions and specific heat capacity of individual phases; (ii) specific heat coupled with thermal expansion, as defined in Eq. (11); (iii) specific heat coupled with moisture migration described as Eq. (16), which includes free water in capillary pores and confined water in gel pores. It is noted that the specific heat of water varies with the pore size, and the specific heat of confined water is only approximately a quarter of the free water, as listed in Table 3. As seen in Fig. 6a, the predicted specific heat of cement paste increases with the w/c ratio after considering the moisture and expansion coupled specific heat, which is in good agreement with the tendency of measured results in Section 4.1.

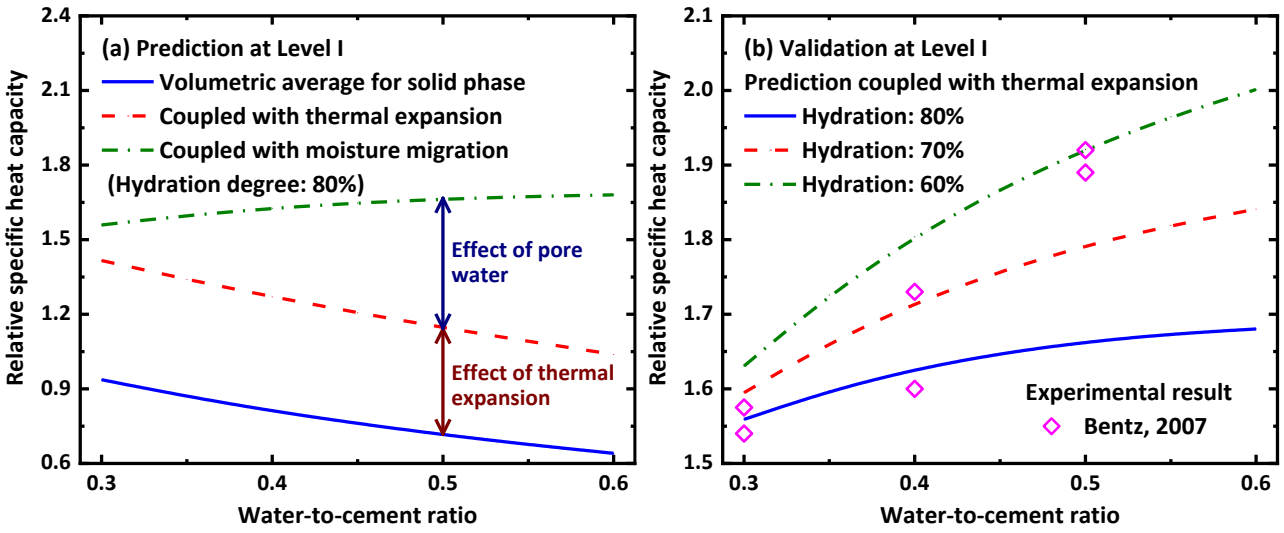

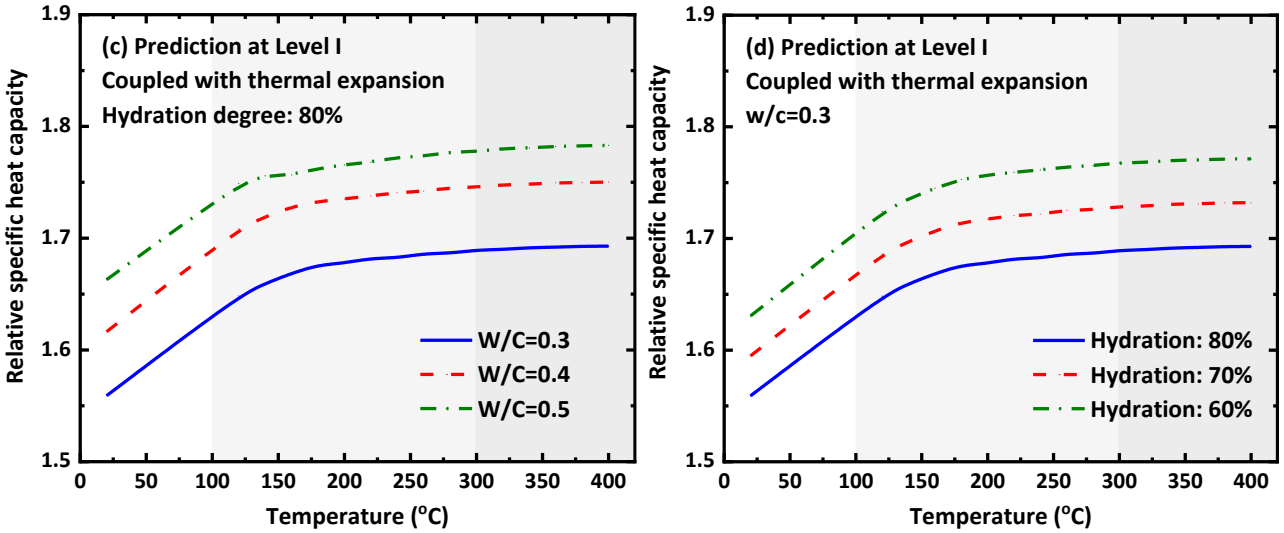

Fig. 6. A comparison of the predicted and measured specific heat of cement paste at Level I.

Fig. 6b presents a comparison of the predicted specific heat capacity of cement paste with the measured data obtained from a previous study [8]. It is clear that most of the measured data lie in the boundary predictions with hydration degrees of 60% and 80%, which is consistent with the previous finding that the hydration degree of cement paste varies from 66% to 77% after curing for 28 d [42], within the w/c ratio range of 0.3–0.5. In order to predict the temperature-dependent specific heat capacity of cement paste, the following two aspects were considered: (i) the decomposition of hydration products would alter the phase composition of cement paste, which was calculated using the dehydration kinetics model given in the Appendix; (ii) the increased specific heat capacity of solid phases with temperature was estimated using the Debye specific heat capacity function (Section 3.3). As such, the specific heat capacity of cement paste at elevated temperatures can be predicted, considering the effects of w/c ratio and hydration degree, the results of which are shown in Fig. 6c and 6d. The growing trend of specific heat capacity with increasing w/c ratio and decreasing hydration degree agrees well with the numerical results presented in Ref. [7].

5.2 Homogenized specific heat capacity at Level II

The homogenized cement paste at Level I, together with fine aggregates, forms the solids phases in the mortar at Level II, the temperature-dependent thermal properties of which can be characterised by the Debye specific heat capacity function, as given in Eq. (14). Towards a better understanding the micro-mechanism of specific heat capacity, a parametric analysis was carried out on the Debye function, including two main variables, i.e., Debye temperature (T_d) and absolute temperature (T). As illustrated in Fig. 7a, the Debye specific heat capacity rises with the increase of absolute temperature, while the growth rate of the Debye function gradually declines with temperature. In contrast, there exists a decreasing trend between Debye specific heat and Debye temperature under

a specific absolute temperature, as displayed in Fig. 7b. In fact, the Debye temperature as an intrinsic thermal parameter of solids generally varies from 373 to 573 K for cementitious composites [40]. Thus, a back-analysis method was applied to estimate the Debye temperature of cement mortar at Level II. To be more specific, the Debye temperature of specimens was calculated by fitting the experimental data with prediction at a specific temperature, and the obtained Debye temperature was employed to predict the specific heat capacity at other temperatures. As such, it is possible to determine the value of Debye temperature, as well as check out whether the Debye temperature of cement mortar changes with absolute temperature. Such method has been proven effective for analysing the physical parameters that are difficult to directly measure [56].

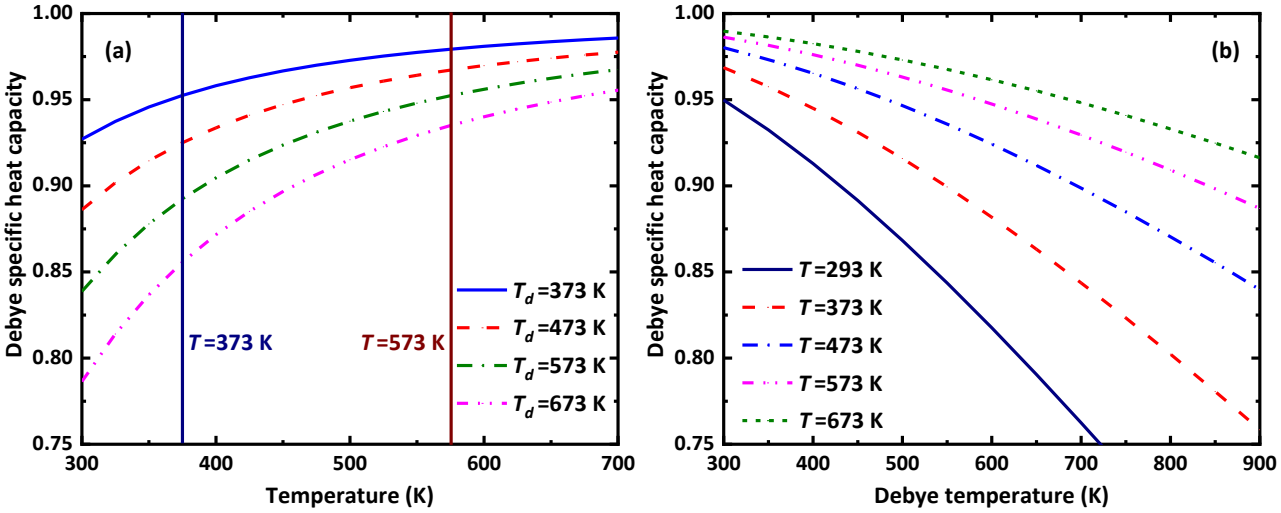

Fig. 7. Debye specific heat capacity against Debye temperature (T_d) and absolute temperature (T).

Fig. 8a shows the predicted specific heat capacity of mortar as a function of the volume fraction of fine aggregate. The effective specific heat capacity of mortar drops when more fine aggregates are incorporated, which can be ascribed to the restraining effect induced by the low specific heat capacity of aggregate [6]. The predictions at elevated temperatures were compared with experimental data, as displayed in Fig. 8b. Take the predictions for mortar with w/c ratio of 0.4 as an example, the experimental data at 100 ^{o}C was adopted as the fitting point, based on which the Debye temperature of around 553 K can be obtained and used for predictions at other temperatures. It can be found that the Debye temperature under a specific w/c ratio is nearly a constant regardless of the absolute temperature and the predictions agree well with experimental results showing the maximum relative difference of 1.6%. This is because the Debye temperature is closely associated with the interfacial thermal properties of solid microstructure, which is highly dependent on the w/c ratio but less relevant to the fine aggregate content, as confirmed by a previous study [57].

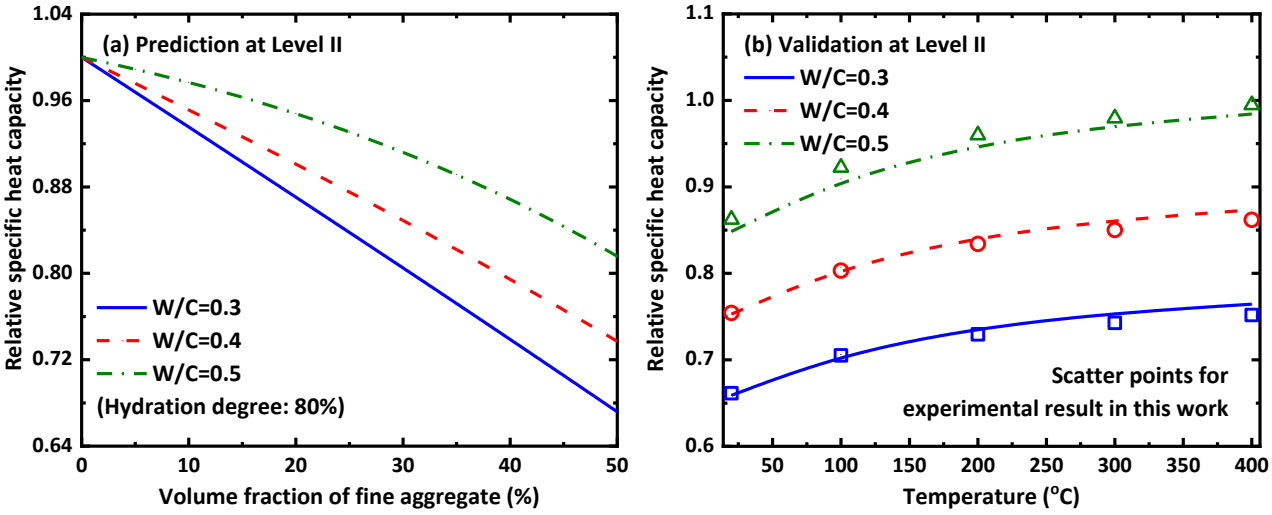

Fig. 8. A comparison of the predicted and measured specific heat of cement mortar at Level II.

5.3 Homogenized specific heat capacity at Level III

At Level III, the aspect ratio of fibre inclusions in the composite exceeds 100, for which the effective thermal properties calculated by homogenization were found to be insensitive to the shape of inclusions [54]. Thus, a simplified calculation method was employed for predictions of fibre reinforced composites by averaging the upper and lower mathematical bounds of the effective specific heat capacity proposed by Rosen and Hashin [58]. Such simplification has been proven effective for estimating the effective properties of hybrid fibre reinforced concrete in previous studies [33,59]. Fig. 9a and 9b show the predicted results for fibre reinforced mortar at elevated temperatures, in comparison with experimental data, indicating a good agreement between predictions and experimental results with a relative difference of only about 3.4%. However, the predicted specific heat capacity of PFRC is lower than that of experimental data, especially at over 300 °C, which can be attributed to the additional specific heat capacity due to the vaporization of PP fibres at around 340 °C. Therefore, the proposed multiscale model still needs further modification to consider the melting and evaporation of polymer fibres.

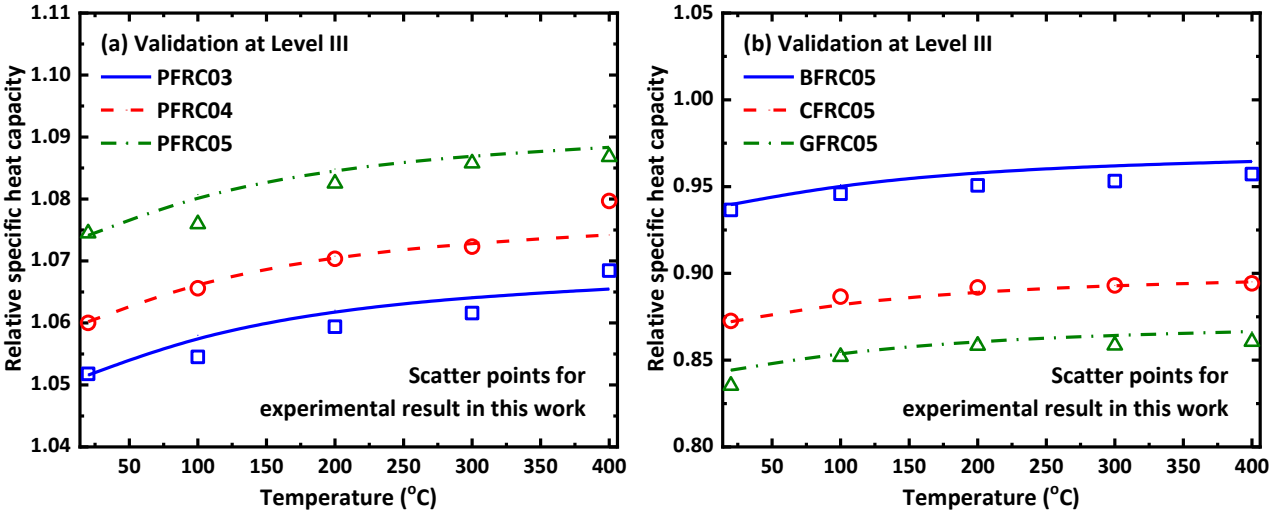

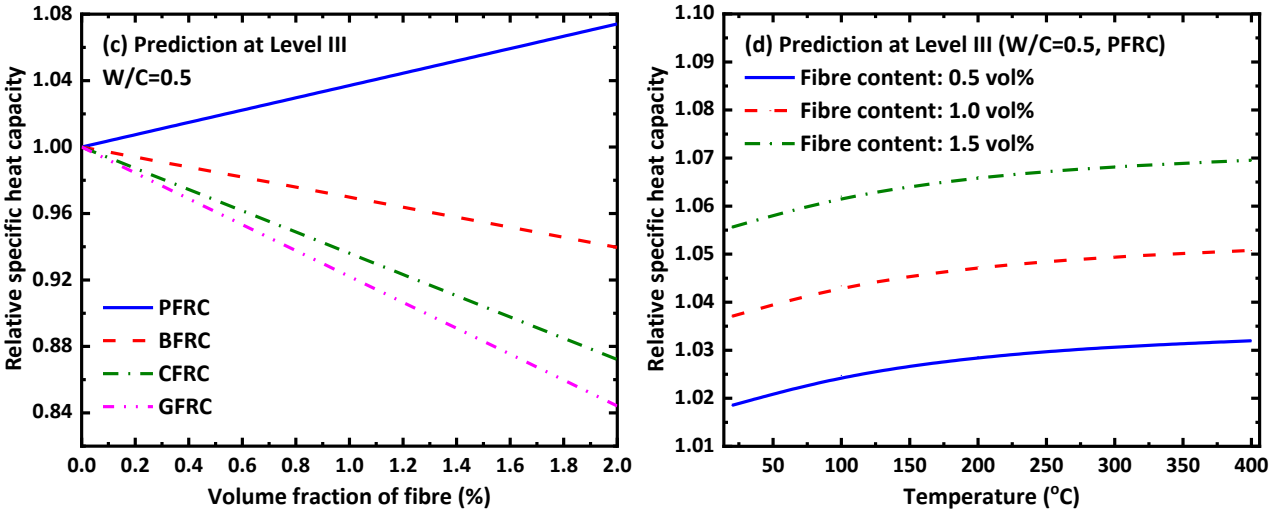

Fig. 9. A comparison of the predicted and measured specific heat capacity of fibre reinforced mortar at Level III.

Fig. 9c presents the predicted specific heat capacity of cement mortar reinforced with various types of fibre as a function of fibre content. From the perspective of composite theory, the specific heat capacity of a multi-phase composite is a function of the thermal properties of its components. Accordingly, fibres with high specific heat capacity (i.e., PP fibres) have a positive effect on the effective specific heat capacity of the composite, while the incorporation of basalt, carbon or glass fibres would restrain the specific heat capacity of the composite due to their low specific heat capacity. In addition, the positive or restraining effect induced by fibre addition can be enhanced when more fibres are incorporated. For example, the addition of 2.0 vol% PP fibre or glass fibre into the mortar with a w/c ratio of 0.5 results in a 3.7% rise or 7.8% drop in relative specific heat. Moreover, as seen in Fig. 9d, the promoting effect of PP fibres under various fibre content can be maintained at elevated temperatures, while the relative specific heat gradually goes up with the increase in temperature. This suggests that hybrid fibres can be adopted to modify the specific heat of cementitious composites and obtain desirable thermal properties at various temperature levels.

6. Parametric analysis

The effective specific heat capacity of multi-phase composite is a critical thermal property, which is not only affected by the specific heat capacity of individual phases but also closely related to the elastic properties and thermal expansion of hybrid inclusions, as discussed in Section 3.2. In order to figure out how and to what extent the mechanical and thermal properties of inclusions would affect the effective specific heat, a parametric analysis was performed on a typical three-phase composite consisting of matrix material (denoted as "*m*") and two types of inclusion (denoted as "*i*" with *i*=1, 2) here. The ratio between the effective property of the composite and the thermal

property of the matrix was used as the relative parameter for comparison and discussion.

6.1 Effective thermal expansion coefficient

For the analysis of thermal expansion, three cases were considered, i.e., the stiffer inclusion case, the softer inclusion case, and the hybrid inclusion case. The former two cases can be simplified to the problem of a two-phase composite, while the volume frictions of the stiffer and softer inclusion are assumed to be the same in the third case. When the stiffer inclusions with bulk modulus and shear modulus five times higher than that of the matrix are incorporated into the composite, the relative thermal expansion coefficient of the composite is plotted as a function of the inclusion content in Fig. 10a. Each line in the curves refers to a specific ratio between the thermal expansion of inclusions and that of the matrix λ_i / λ_m, varying from 0.2 to 5.0. In general, the high expansion of inclusions would lead to a promoting effect on the effective thermal expansion, while the low expansion of inclusions can result in a restraining effect on the composite. For instance, the composite with 10% high expansion inclusions (λ_i / λ_m = 5.0) or low expansion inclusions (λ_i / λ_m = 0.2) has a 26.2% rise or 5.2% drop in effective thermal expansion coefficient, compared to the reference matrix.

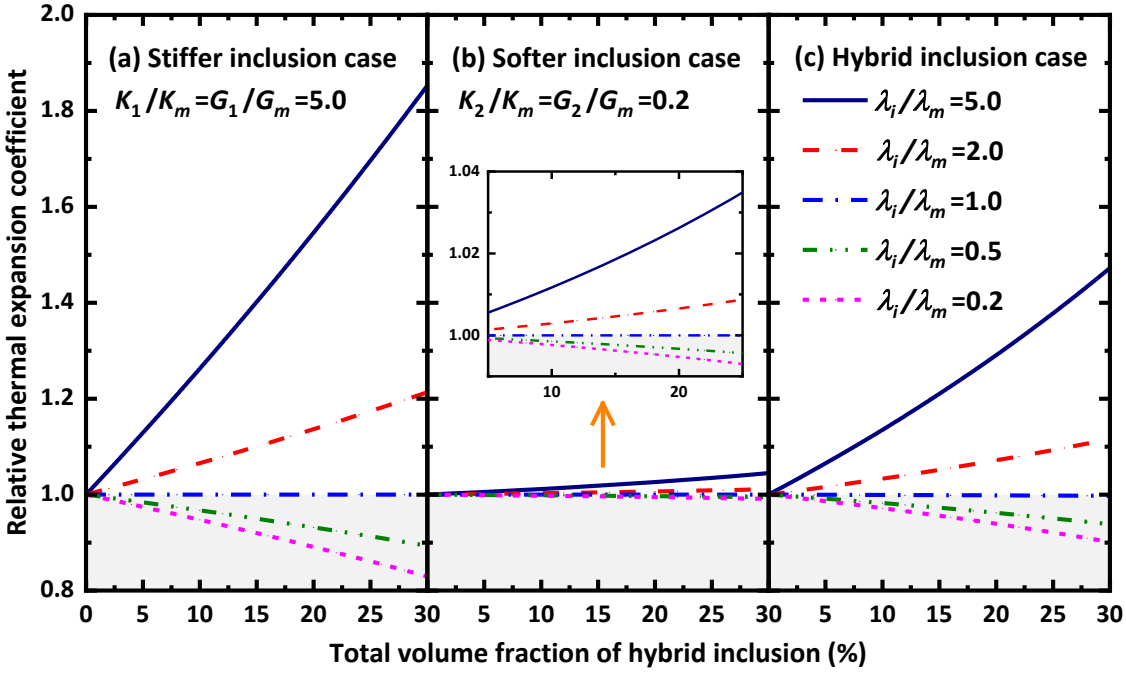

Fig. 10. Effective thermal expansion coefficient of the composite with various inclusions.

Fig. 10b presents the predictions for the case that the inclusions are softer with the bulk modulus and shear modulus only one-fifth lower than that of the matrix. In contrast with the stiffer inclusion case, the promoting or restraining effect of the high or low expansion of inclusions is significantly weakened due to the low modulus of inclusions. For the high expansion condition with λ_i / λ_m = 2.0, the incorporation of 20% stiffer inclusions would induce a 36.43% increase in relative thermal

expansion coefficient, while only a 0.66% rise can be obtained in the softer case. In addition, when the thermal expansion of inclusions is equal to that of the matrix, the relative thermal expansion coefficient maintains at 1.0, regardless of the modulus of inclusions.

Fig. 10c shows the predictions of the hybrid inclusion case, indicating that stiffer inclusions play the dominant role in determining the relative thermal expansion when the same volume fraction of stiffer and softer inclusions are incorporated. In other words, the higher (or lower) the thermal expansion of the stiffer inclusions, the more enhanced the promoting (or restraining) effect on the effective thermal property, while the prediction results are insensitive to the thermal expansion of the softer inclusions. Moreover, the addition of inclusions with the same thermal expansion as the matrix material does not influence the relative thermal expansion.

6.2 Effective specific heat capacity coupled with thermal expansion

The expansion coupled specific heat capacity of a multi-phase composite was estimated under three types of cases in accordance with the analysis of effective thermal expansion. For each case, two sets of specific heat capacity ratios between inclusions and matrix (C_i / C_m) were adopted, including a higher capacity condition of C_i / C_m = 1.6, and a lower capacity condition of C_i / C_m = 0.4. In addition, three sets of thermal expansion ratios (λ_i / λ_m) varying from 0.5 to 2.0 were considered.

Fig. 11a plots the predicted results for the stiffer inclusion case in terms of the relative specific heat capacity as a function of inclusion content. Overall, the stiffer inclusions with higher thermal expansion and specific heat capacity have a promoting effect on the relative specific heat capacity, while the promoting effect of high thermal expansion can even play a more important role under given conditions. For instance, the addition of 10% inclusions with lower specific heat capacity can still lead to a significant increase of 41.5% in relative specific heat capacity, when the thermal expansion coefficient of inclusions is double higher than that of the matrix. Moreover, the promoting effect induced by higher capacity or higher expansion of inclusions can compensate for the restraining effect due to the inferior thermal properties. To be more specific, there is still a 12.6% rise in the relative specific heat capacity by incorporating higher capacity inclusions with a lower thermal expansion ratio (λ_i / λ_m) of 0.5. Additionally, the predictions for stiffer inclusion cases have a wide variation range from 0.82 to 2.11, suggesting that stiffer inclusions can effectively alter the thermal properties of the composite.

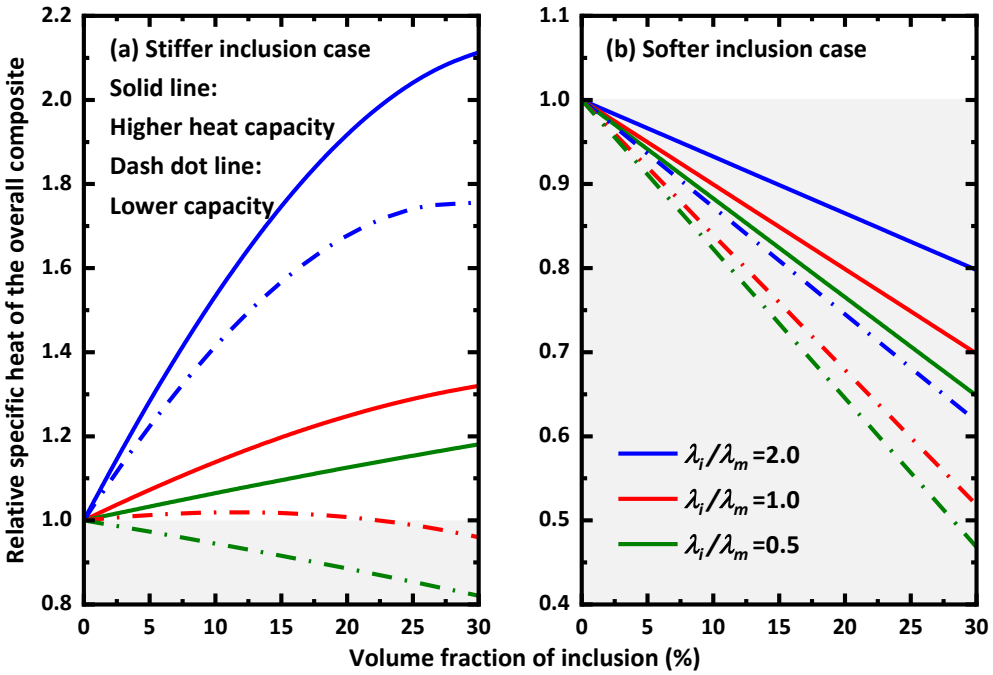

Fig. 11. Relative specific heat capacity of the composite with stiffer or softer inclusions.

For the softer inclusion case, the promoting effect of higher capacity or higher expansion inclusions would be greatly reduced, as plotted in Fig. 11b. The relative specific heat capacity of the overall composite is even 6.74% lower than the specific heat capacity of the matrix material when adding 10% inclusions with C_i / C_m = 1.6 and λ_i / λ_m = 2.0. This implies that the incorporation of inclusions with lower elastic modulus tends to restrain the effective thermal property of the composite. Accordingly, extremely high thermal parameters of inclusions are required to enhance the thermal performance of the composite with softer inclusions. For instance, the experimental results presented in Section 4.2 indicate that the low-modulus PP fibres can enhance the specific heat capacity of cementitious composites, as the linear thermal expansion coefficient of PP fibres is approximately an order of magnitude higher than that of cement paste [60].

Fig. 12 displays the predictions for hybrid inclusions cases with the volume ratio between stiffer and softer inclusions varying from 2.0 to 0.5. It is obvious that the incorporation of softer inclusions would weaken the promoting effect of stiffer inclusions on the effective specific heat capacity of the overall composite, and the weakening degree goes up with the rising content of softer inclusions. For instance, the relative specific heat capacity reaches as high as 1.75 when adding 15% stiffer inclusions, in comparison with that of 1.52 when adding hybrid 10% stiffer inclusions and 5% softer inclusions, while the thermal expansion ratio is maintained at 2.0. Moreover, the maximum value of the predicted relative specific heat capacity gradually declines from 1.93 to 1.38 when the volume ratio between stiffer and softer inclusions drops from 2.0 to 0.5. In contrast, the change in the mix proportion of hybrid inclusions has a minor effect on the

prediction for composites with lower expansion inclusions. To be more specific, the minimum relative specific heat capacity maintains at around 0.84–0.88, regardless of the composition of inclusions, when the thermal expansion coefficient of inclusions is half of the matrix.

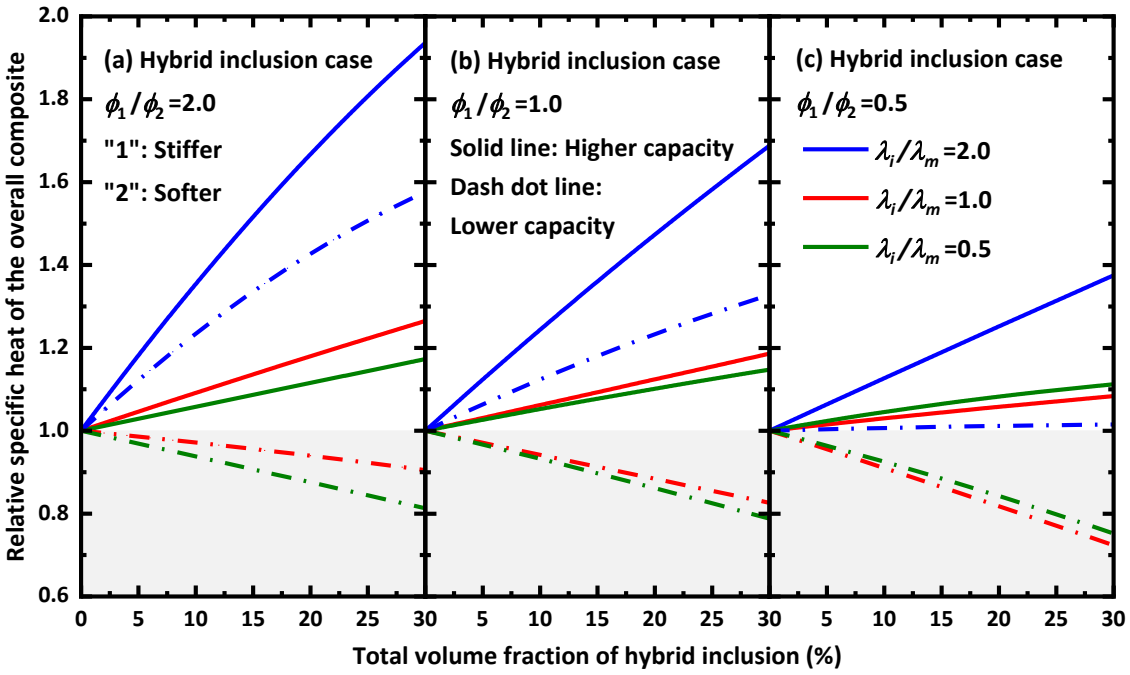

Fig. 12. Relative specific heat capacity of the composite with hybrid inclusions.

As indicated in Eq. (11), the overall effective specific heat capacity is composed of two parts, including the volumetric average part and the thermal expansion coupled part. Fig. 13 shows the contribution of thermal expansion coupled specific heat capacity to the overall effective specific heat capacity of the composite. It can be found that the thermal expansion coupled specific heat capacity for stiffer inclusion case reduces significantly from 45.4% to 0.90% under inclusion content of 20%, while that for softer inclusion case only slightly drops from -6.8% to -10.0%, with the decreasing λ_i / λ_m from 2.0 to 0.5. This indicates that the higher the specific heat capacity of the stiffer inclusions, the more sensitive the thermal expansion coupled specific heat capacity to the thermal expansion coefficient. In addition, the predictions for the softer inclusion case are insensitive to the variation of the thermal expansion coefficient. The above analysis suggests that high-modulus inclusions (i.e., basalt, carbon and glass fibres) seem to be more effective in altering the overall effective specific heat capacity if given higher specific heat capacity or thermal expansion through physical or chemical methods. Moreover, although the elastic modulus of polymer fibres is inferior to cement paste, the high thermal expansion of PP fibres still makes it a feasible solution to enhance the effective thermal properties, as illustrated in Fig. 14.

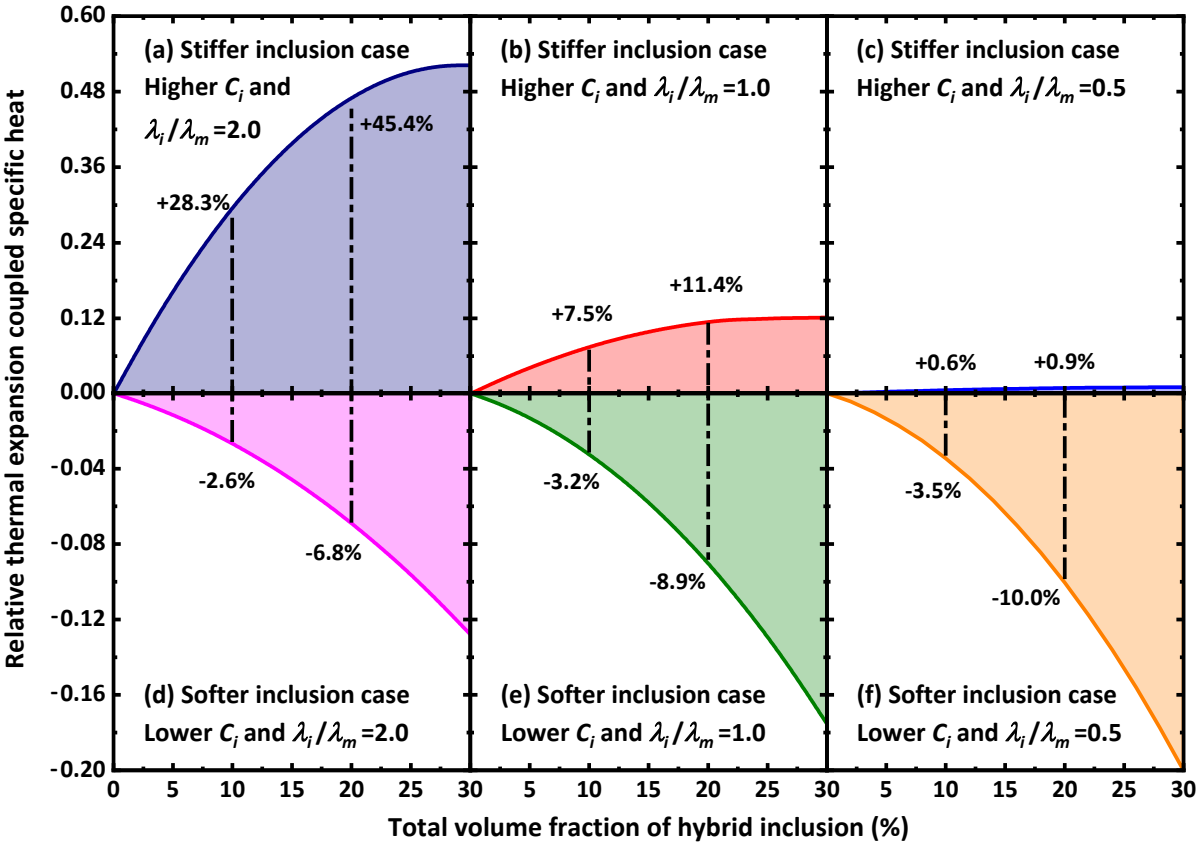

Fig. 13. Effect of thermal expansion coupled specific heat on the overall specific heat capacity.

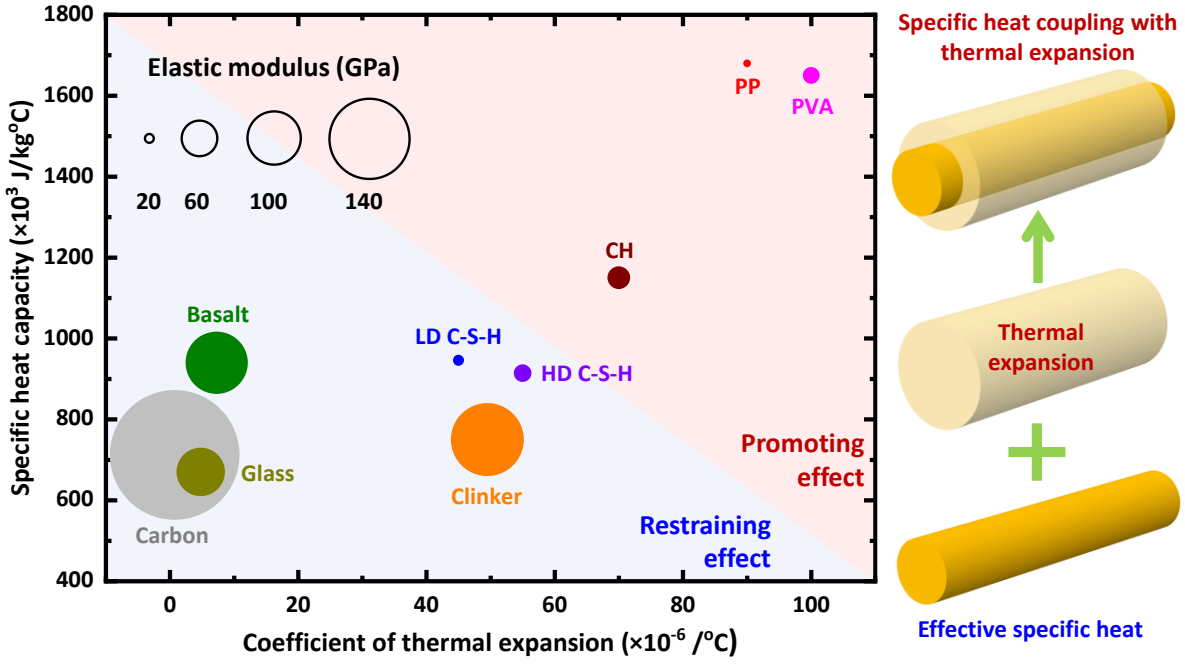

Fig. 14. Illustration of the thermal expansion coupled specific heat capacity of inclusions in cementitious composites (Note: PVA denotes polyvinyl alcohol).

7. Conclusions

In this study, the role of four types of micro fibres in the specific heat capacity of cement mortar at elevated temperatures was systematically investigated based on a series of experimental

measurements, micromechanical modelling and parametric analysis. Based on the results obtained, the main conclusions can be drawn as follows:

(1) The specific heat capacity of cement mortar goes up with the increase of w/c ratio and temperature, which can be attributed to the increased moisture content and the moisture evaporation and improved specific heat capacity of solids, respectively. The effect of the w/c ratio on specific heat capacity is maintained at elevated temperatures, as there exists only about a 16.4% difference in specific heat capacity when the w/c ratio varies from 0.3 to 0.5 at 400 ^{o}C.

(2) The addition of PP fibres can enhance the specific heat capacity of mortar because of the high specific heat capacity of polymer at ambient temperature, while the thermal expansion and melting of PP fibres further contribute to the additional specific heat capacity of mortar at elevated temperatures. In contrast, the low specific heat capacity of basalt, carbon and glass fibres has a restraining effect on the specific heat capacity of mortar. The incorporation of 2.0 vol% PP or glass fibres leads to the maximum rise or drop in specific heat capacity of mortar by 8.9% and 14.1% respectively over the measured temperatures.

(3) A multiscale thermo-mechanical specific heat capacity model was developed for multi-phase composites, considering the thermal expansion coupling effect, Debye specific heat capacity function and moisture migration. The effective specific heat capacity of cementitious composites predicted using the proposed model through step-by-step homogenization from cement paste level to fibre reinforced mortar level shows a good agreement well with the experimental data at up to 400 ^{o}C, with the maximum relative difference of less than 5.0%.

(4) The parametric analyses on three-phase composites reveal that the stiffer inclusions govern the effective specific heat capacity coupling with thermal expansion, while the composite with softer inclusions is insensitive to the variation in thermal properties of inclusions. For a stiffer inclusion case, the higher the thermal expansion and specific heat capacity of inclusions, the more enhanced the thermal expansion coupled specific heat capacity of the composite. For the softer inclusion case, the higher specific heat capacity of inclusions might not guarantee the promoting effect on the specific heat capacity of the composite, unless an extremely high thermal expansion coefficient of inclusions is achieved.

Appendix A

The low order terms of Debye specific heat capacity function in Eq. (14) can be estimated through Taylor series expansion as [40]:

$$G(\delta)=\frac{3}{\delta^3}\int_0^{\delta}\frac{\delta^4 e^{\delta}}{\left(e^{\delta}-1\right)^2}d\delta \tag{A1}$$

$$G'(\delta)=-\frac{9}{\delta^4}\int_0^{\delta}\frac{\vartheta^4 e^{\delta}}{\left(e^{\delta}-1\right)^2}d\delta+\frac{3\delta e^{\delta}}{\left(e^{\delta}-1\right)^2} \tag{A2}$$

$$G''(\delta)=\frac{36}{\delta^5}\int_0^{\delta}\frac{\delta^4 e^{\delta}}{\left(e^{\delta}-1\right)^2}d\delta+\frac{3\delta e^{\delta}-6e^{\delta}}{\left(e^{\delta}-1\right)^2}-\frac{6\delta e^{2\delta}}{\left(e^{\delta}-1\right)^2} \tag{A3}$$

$$G'''(\delta)=-\frac{180}{\delta^6}\int_0^{\delta}\frac{\delta^4 e^{\delta}}{\left(e^{\delta}-1\right)^2}d\delta+\frac{36e^{\delta}}{\delta\left(e^{\delta}-1\right)^2}+\frac{3\delta e^{\delta}-3e^{\delta}}{\left(e^{\delta}-1\right)^2}-\frac{18\delta e^{2\delta}-6e^{2\delta}}{\left(e^{\delta}-1\right)^3}+\frac{18\delta e^{3\delta}}{\left(e^{\delta}-1\right)^4} \tag{A4}$$

Appendix B

In order to determine the dehydrated moisture in Eq. (16), the kinetics model of hydrates dehydration was adopted in a generalized form [50]:

$$\ln\left(\frac{d\alpha_i}{dt}\right)=-\frac{E_{a,i}}{R\cdot T(t)}+\ln\beta_i+\ln\left(1-\alpha_i\right) \tag{B1}$$

where α_i, $E_{a,i}$ and β_i denote the dehydration degree, activation energy and pre-exponential factor of hydrated phase *i*, respectively, *R* is the universal gas constant of 8.314 J/(mol·K), and *t* stands for the time.

Acknowledgements

This study was funded by the National Natural Science Foundation of China (Nos. 52178382 and 52078378), the Fundamental Research Funds for the Central Universities (No. N2201023) and the Natural Science Funds of Liaoning Province (No. 2020-MS-089). M. Zhang gratefully acknowledges the financial support from the Engineering and Physical Sciences Research Council (EPSRC), UK under Grant No. EP/R041504/1 and the Royal Society, UK under Award No. IEC\NSFC\191417.

References

[1] H.R. Pakravan, M. Latifi, M. Jamshidi, Hybrid short fiber reinforcement system in concrete: A review, Constr. Build. Mater. 142 (2017) 280–294. https://doi.org/10.1016/j.conbuildmat.2017.03.059.

[2] P. Sha, I. Asadi, P. Shafigh, I. Asadi, N.B. Mahyuddin, P. Sha, I. Asadi, Concrete as a thermal mass material for building applications - A review, J. Build. Eng. 19 (2018) 14–25. https://doi.org/10.1016/j.jobe.2018.04.021.

[3] T. Zhang, M. Zhang, Y. Shen, H. Zhu, Z. Yan, Mitigating the damage of ultra-high performance concrete at elevated temperatures using synergistic flame-retardant polymer fibres, Cem. Concr. Res. 158 (2022) 106835. https://doi.org/10.1016/J.CEMCONRES.2022.106835.

[4] Y. Wang, C. Ma, Y. Liu, D. Wang, J. Liu, A model for the effective thermal conductivity of moist porous building materials based on fractal theory, Int. J. Heat Mass Transf. 125 (2018) 387–399. https://doi.org/10.1016/j.ijheatmasstransfer.2018.04.063.

[5] S. Xu, J. Liu, Q. Zeng, Towards better characterizing thermal conductivity of cement-based materials: The effects of interfacial thermal resistance and inclusion size, Mater. Des. 157 (2018) 105–118. https://doi.org/10.1016/j.matdes.2018.07.034.

[6] Y. Xu, D.D.L. Chung, Effect of sand addition on the specific heat and thermal conductivity of cement, Cem. Concr. Res. 30 (2000) 59–61. https://doi.org/10.1016/S0008-8846(99)00206-9.

[7] T. Honorio, B. Bary, F. Benboudjema, Thermal properties of cement-based materials : Multiscale estimations at early-age, Cem. Concr. Compos. 87 (2018) 205–219. https://doi.org/10.1016/j.cemconcomp.2018.01.003.

[8] D.P. Bentz, Transient plane source measurements of the thermal properties of hydrating cement pastes, Mater. Struct. 40 (2007) 1073–1080. https://doi.org/10.1617/s11527-006-9206-9.

[9] K.-Y. Shin, S.-B. Kim, J.-H. Kim, M. Chung, P.-S. Jung, Thermo-physical properties and transient heat transfer of concrete at elevated temperatures, Nucl. Eng. Des. 212 (2002) 233–241. https://doi.org/10.1016/S0029-5493(01)00487-3.

[10] Y. Shen, H. Zhu, Z. Yan, L. Zhou, T. Zhang, Y. Men, Y. Lu, Thermo-mechanical analysis of fire effects on the structural performance of shield tunnels, Tunn. Undergr. Sp. Technol. 132 (2023) 104885. https://doi.org/10.1016/j.tust.2022.104885.X.

[11] M. Briffaut, F. Benboudjema, J.M. Torrenti, G. Nahas, Effects of early-age thermal behaviour on damage risks in massive concrete structures, Eur. J. Environ. Civ. Eng. 16 (2012) 589–605. https://doi.org/10.1080/19648189.2012.668016.

[12] I. Asadi, P. Shafigh, Z.F. Bin Abu Hassan, N.B. Mahyuddin, Thermal conductivity of concrete – A review, J. Build. Eng. 20 (2018) 81–93. https://doi.org/10.1016/j.jobe.2018.07.002.

[13] N. Ranjbar, M. Zhang, Fiber-reinforced geopolymer composites : A review, Cem. Concr. Compos. 107 (2020) 103498. https://doi.org/10.1016/j.cemconcomp.2019.103498.

[14] M. Chen, J. Feng, Y. Cao, T. Zhang, Synergetic effects of hybrid steel and recycled tyre polymer fibres on workability, mechanical strengths and toughness of concrete, Constr. Build. Mater. 368 (2023) 130421. https://ddoi.org/10.1016/j.conbuildmat.2023.130421.

[15] M. Chen, H. Si, X. Fan, Y. Xuan, M. Zhang, Dynamic compressive behaviour of recycled tyre steel fibre reinforced concrete, Constr. Build. Mater. 316 (2022) 125896. https://doi.org/10.1016/j.conbuildmat.2021.125896.

[16] P. Nuaklong, N. Boonchoo, P. Jongvivatsakul, T. Charinpanitkul, P. Sukontasukkul, Hybrid effect of carbon nanotubes and polypropylene fibers on mechanical properties and fire resistance of cement mortar, Constr. Build. Mater. 275 (2021) 122189. https://doi.org/10.1016/J.CONBUILDMAT.2020.122189.

[17] A. Schwartzentruber, M. Philippe, G. Marchese, Effect of PVA, glass and metallic fibers, and of an expansive admixture on the cracking tendency of ultrahigh strength mortar, Cem. Concr. Compos. 26 (2004) 573–580. https://doi.org/10.1016/S0958-9465(03)00076-3.

[18] F. Koksal, E.T. Kocabeyoglu, O. Gencel, A. Benli, The effects of high temperature and cooling regimes on the mechanical and durability properties of basalt fiber reinforced mortars with silica fume, Cem. Concr. Compos. 121 (2021) 104107. https://doi.org/10.1016/J.CEMCONCOMP.2021.104107.

[19] F.J. Baeza, O. Galao, I.J. Vegas, M. Cano, P. Garcés, Influence of recycled slag aggregates on the conductivity and strain sensing capacity of carbon fiber reinforced cement mortars, Constr. Build. Mater. 184 (2018) 311–319. https://doi.org/10.1016/J.CONBUILDMAT.2018.06.218.

[20] Y. Yao, B. Wang, Y. Zhuge, Z. Huang, Properties of hybrid basalt-polypropylene fiber reinforced mortar at different temperatures, Constr. Build. Mater. 346 (2022) 128433. https://doi.org/10.1016/j.conbuildmat.2022.128433.

[21] V.K.R. Kodur, P.P. Bhatt, M.Z. Naser, High temperature properties of fiber reinforced polymers and fire insulation for fire resistance modeling of strengthened concrete structures, Compos. Part B. 175 (2019) 107104. https://doi.org/10.1016/j.compositesb.2019.107104.

[22] R. Borinaga-Treviño, A. Orbe, J. Canales, J. Norambuena-Contreras, Thermal and mechanical properties of mortars reinforced with recycled brass fibres, Constr. Build. Mater. 284 (2021) 122832. https://doi.org/10.1016/J.CONBUILDMAT.2021.122832.

[23] T. Zhang, Y. Zhang, H. Zhu, Z. Yan, Experimental investigation and multi-level modeling of the effective thermal conductivity of hybrid micro-fiber reinforced cementitious composites at elevated temperatures, Compos. Struct. 256 (2021) 112988. https://doi.org/10.1016/j.compstruct.2020.112988.

[24] V. Kodur, S. Banerji, R. Solhmirzaei, Effect of temperature on thermal properties of ultrahigh-performance concrete, J. Mater. Civ. Eng. 32 (2020) 04020210. https://doi.org/10.1061/(ASCE)MT.1943-5533.0003286.

[25] Q. Zeng, R. Fang, H. Li, Y. Peng, J. Wang, Tailoring the thermal and mechanical properties of lightweight cement-based composites by macro and micro fillers, Cem. Concr. Compos. 102 (2019) 169–184. https://doi.org/10.1016/j.cemconcomp.2019.04.014.

[26] Y.K. Park, J. Lee, J. Kim, A new approach to predict the thermal conductivity of composites with coated spherical fillers and imperfect interface, Mater. Trans. 49 (2008) 733–736. https://doi.org/10.2320/matertrans.MRA2007135.

[27] T. Zhang, H. Zhu, C. Guo, Z. Yan, Tailoring the thermal conductivity of functional cementitious composites with micro core-shell particles: A multiscale homogenization study, Constr. Build. Mater. 300 (2021) 124289. https://doi.org/10.1016/j.conbuildmat.2021.124289.

[28] GB/T 50081, Chinese code for test methods of concrete physical and mechanical properties,

Beijing, (2019).
[29] ISO 22007-2, Plastics-Determination of thermal conductivity and thermal diffusivity, Geneva, (2015).
[30] Permanent International Association of Road Congresses, Proposal on the Design Criteria for Resistance to Fire for Road Tunnel Structures, PIARC, Paris, (2012).
[31] J. Lee, Y. Xi, K. Willam, Y. Jung, A multiscale model for modulus of elasticity of concrete at high temperatures, Cem. Concr. Res. 39 (2009) 754–762. https://doi.org/10.1016/j.cemconres.2009.05.008.
[32] H. Li, Q. Zeng, S. Xu, Effect of pore shape on the thermal conductivity of partially saturated cement-based porous composites, Cem. Concr. Compos. 81 (2017) 87–96. https://doi.org/10.1016/j.cemconcomp.2017.05.002.
[33] Q. Chen, H. Zhu, Z. Yan, J.W. Ju, Z. Jiang, Y. Wang, A multiphase micromechanical model for hybrid fiber reinforced concrete considering the aggregate and ITZ effects, Constr. Build. Mater. 114 (2016) 839–850. https://doi.org/10.1016/j.conbuildmat.2016.04.008.
[34] L. V. Gibiansky, S. Torquato, Thermal expansion of isotropic multiphase composites and polycrystals, J. Mech. Phys. Solids. 45 (1997) 1223–1252. https://doi.org/10.1016/S0022-5096(96)00129-9.
[35] V.M. Levin, Thermal expansion coefficients of heterogeneous materials, Lzu Akad Nauk SSSR Mekh Tuerd Tela. 2 (1967) 88–94. https://doi.org/10.1063/1.1735842.
[36] I. Sevostianov, M. Kachanov, Connections between Elastic and Conductive Properties of Heterogeneous Materials, Adv. Appl. Mech. 42 (2009) 69–252. https://doi.org/10.1016/S0065-2156(08)00002-1.
[37] Y. Benveniste, A new approach to the application of Mori-Tanaka's theory in composite materials, Mech. Mater. 6 (1987) 147–157. https://doi.org/10.1016/0167-6636(87)90005-6.
[38] J.D. Eshelby, The determination of the elastic field of an ellipsoidal inclusion, and related problems, Proc. R. Soc. Lond. A. Math. Phys. Sci. 241 (1957) 376–396. https://doi.org/10.1017/S0305004100053366.
[39] M.X. Gu, C.Q. Sun, Z. Chen, T.C. Au Yeung, S. Li, C.M. Tan, V. Nosik, Size, temperature, and bond nature dependence of elasticity and its derivatives on extensibility, Debye temperature, and heat capacity of nanostructures, Phys. Rev. B - Condens. Matter Mater. Phys. 75 (2007) 1–9. https://doi.org/10.1103/PhysRevB.75.125403.
[40] Y. Ju, H. Liu, J. Liu, K. Tian, S. Wei, S. Hao, Investigation on thermophysical properties of reactive powder concrete, Sci. China Technol. Sci. 54 (2011) 3382–3403. https://doi.org/10.1007/s11431-011-4536-4.
[41] C.N. Ang, Y.C. Wang, The effect of water movement on specific heat of gypsum plasterboard in heat transfer analysis under natural fire exposure, Constr. Build. Mater. 18 (2004) 505–515.

https://doi.org/10.1016/j.conbuildmat.2004.04.003.

[42] H.S. Wong, N.R. Buenfeld, Determining the water-cement ratio, cement content, water content and degree of hydration of hardened cement paste: Method development and validation on paste samples, Cem. Concr. Res. 39 (2009) 957–965. https://doi.org/10.1016/j.cemconres.2009.06.013.

[43] V.K.R. Kodur, Properties of Concrete at Elevated Temperatures, ISRN Civ. Eng. 2014 (2014) 1–15. https://doi.org/10.1155/2014/468510.

[44] G.A. Khoury, Effect of fire on concrete and concrete structures, Prog. Struct. Eng. Mater. 2 (2000) 429–447. https://doi.org/10.1002/pse.51.

[45] Design of concrete structures, Eurocode 2, Part 1-2: Structure Fire Design, 2004.

[46] Y. Chen, Y. Zhang, S. Zhang, Q. Guo, Y. Gao, T. Zhang, W. Zhao, Q. Chen, H. Zhu, Experimental study on the thermal properties of a novel ultra-high performance concrete reinforced with multi-scale fibers at elevated temperatures, Constr. Build. Mater. 366 (2023) 130229. https://doi.org/10.1016/J.CONBUILDMAT.2022.130229.

[47] V. Kodur, Properties of Concrete at Elevated Temperatures, ISRN Civ. Eng. 2014 (2014) 1–15. https://doi.org/10.1155/2014/468510.

[48] V.K.R. Kodur, S. Banerji, R. Solhmirzaei, Test methods for characterizing concrete properties at elevated temperature, Fire Mater. (2019) 1–15. https://doi.org/10.1002/fam.2777.

[49] M. Javad, A. Qomi, F. Ulm, R.J. Pellenq, Physical origins of thermal properties of cement paste, Phys. Rev. Appl. 3 (2015) 064010. https://doi.org/10.1103/PhysRevApplied.3.064010.

[50] Q. Zhang, G. Ye, Dehydration kinetics of Portland cement paste at high temperature, J. Therm. Anal. Calorim. 110 (2012) 153–158. https://doi.org/10.1007/s10973-012-2303-9.

[51] G.A. Khoury, Strain of heated concrete during two thermal cycles. Part 1: Strain over two cycles, during first heating and at subsequent constant temperature, Mag. Concr. Res. 58 (2006) 367–385. https://doi.org/10.1680/macr.2006.58.6.367.

[52] Y. Zhang, S. Zhang, X. Jiang, Q. Chen, Z. Jiang, J.W. Ju, M. Bauchy, Insights into the thermal effect on the fracture toughness of calcium silicate hydrate grains: A reactive molecular dynamics study, Cem. Concr. Compos. 134 (2022) 104824. https://doi.org/10.1016/J.CEMCONCOMP.2022.104824.

[53] P.D. Tennis, H.M. Jennings, A model for two types of calcium silicate hydrate in the microstructure of Portland cement pastes, Cem. Concr. Res. 30 (2000) 855–863. https://doi.org/10.1016/S0008-8846(00)00257-X.

[54] T. Zhang, Y. Zhang, H. Zhu, Z. Yan, Characterizing the thermal properties of hybrid polypropylene-steel fiber reinforced concrete under heat exposure: Insights into fiber geometry and orientation distribution, Compos. Struct. 275 (2021) 114457. https://doi.org/10.1016/j.compstruct.2021.114457.

[55] S. Xu, G.W. Scherer, T.S. Mahadevan, S.H. Garofalini, Thermal expansion of confined water, Langmuir. 25 (2009) 5076–5083. https://doi.org/10.1021/la804061p.

[56] S. Liang, Y. Wei, Imperfect interface effect on creep property of hardened-cement pastes: investigations from nano to micro scales, J. Mater. Civ. Eng. 32 (2020) 1–16. https://doi.org/10.1061/(ASCE)MT.1943-5533.0003238.

[57] S. Liang, Y. Wei, Z. Wu, Multiscale modeling elastic properties of cement-based materials considering imperfect interface effect, Constr. Build. Mater. 154 (2017) 567–579. https://doi.org/10.1016/j.conbuildmat.2017.07.196.

[58] B.W. Rosen, Z. Hashin, Effective thermal expansion coefficients and specific heats of composite materials, Int. J. Eng. Sci. 8 (1970) 157–173. https://doi.org/10.1016/0020-7225(70)90066-2.

[59] Y. Zhang, J.W. Ju, H. Zhu, Z. Yan, A novel multi-scale model for predicting the thermal damage of hybrid fiber-reinforced concrete, Int. J. Damage Mech. 29 (2019) 19–44. https://doi.org/10.1177/1056789519831554.

[60] G.A. Khoury, B. Willoughby, Polypropylene fibres in heated concrete. Part 1: Molecular structure and materials behaviour, Mag. Concr. Res. 60 (2008) 125–136. https://doi.org/10.1680/macr.2008.60.2.125.